Physics – Uspekhi **47** (12) 1177 – 1203 (2004)

REVIEWS OF TOPICAL PROBLEMS PACS numbers: 42.25.Bs, 42.30.Lr, 42.60.Jf

Spiral light beams

E G Abramochkin, V G Volostnikov

DOI: 10.1070/PU2004v047n12ABEH001802

Contents

Abstract. This paper discusses theoretical and experimental results of the investigation of light beams that retain their intensity structure during propagation and focusing. We describe a family of laser beams termed spiral whose intensity remains invariable, up to scale and rotation, during propagation. Several properties of spiral beams are of practical interest for laser technologies, medicine, and microbiology. The problem of synthesis of spiral beams with the intensity distribution given by an arbitrary planar curve is considered. We emphasize the feasibility, in principle, of making lasers that directly generate beams with desired properties without additional unconventional optics.

1. Introduction

It is well known that the propagation of a light field is a wave phenomenon and, like any oscillatory process, is characterized by a complex-valued amplitude. When the distribution of a complex field amplitude is defined in some plane, the subsequent field evolution in the course of its propagation is described by some differential equation. Hence, it follows that the light field, generally speaking, undergoes quantitative and qualitative changes.

However, with the discovery of lasers and the advent of coherent optics describing the propagation of laser beams, it was theoretically and experimentally shown that lasers can radiate light beams that are self-consistent such that they retain, up to scale, their structure during propagation and focusing [2]. Such beams are the eigenmodes of laser resonators, have a strictly defined form, and are described by two families of special functions with different types of symmetry: Hermite – Gauss and Laguerre – Gauss beams. The lowest oscillation type in these families is the same and is the well-known two-dimensional Gaussian function. Retention of the structure of these beams during their propagation and focusing may be associated with uniform tensile – compressive deformations: convergent and divergent beams.

This brings up the legitimate question: Is there some optical analogy to a torsional strain for beams with a nonuniform divergence or a complicated phase distribution? It turns out that this analogy is justified owing to the generally vortical character of the vector field of light energy flux. This was shown in Refs [3, 4], which were concerned with the investigation of the interrelation between the energy and phase properties of a two-dimensional wave field in the Fresnel zone.

This formulation of the problem is due to the specific character of the optical range, whereby amenable to recording is not the complex amplitude of the optical signal but only its intensity, which is not a complete characteristic of the light field in general. Traditional interferometric techniques allow indirect phase measurements. But in a number of problems, it is impossible or difficult to realize the interferometric principle of obtaining information on the complex amplitude or phase of the field. The problem of recovering the phase information from intensity measurements is known as the phase retrieval problem in optics. This situation occurs, for instance, in astronomy and in X-ray and adaptive optics.

In this connection, the problem of how many and what additional intensity measurements should be made to gain complete information on the field was investigated in [3, 4].

E G Abramochkin, V G Volostnikov Samara Branch of the Lebedev Physics Institute, Russian Academy of Sciences,
ul. Novo-Sadovaya 221, 443011 Samara, Russian Federation
Tel. (7-8462) 34-73-96, (7-8462) 35-56-00
E-mail: coherent@fian.smr.ru, ega@fian.smr.ru

Received 22 January 2004, revised 24 June 2004
Uspekhi Fizicheskikh Nauk **174** (12) 1273 – 1300 (2004)
Translated by E N Ragozin; edited by A M Semikhatov

Because the field changes during propagation, the natural problem setting consists in the field reconstruction from the intensity and the directional derivative taken in the direction of propagation. A comparative analysis of this problem for two- and one-dimensional fields revealed a radical difference between these two cases. It turned out that the problem for a two-dimensional light field reduces to the reconstruction of the vector field of light energy flux from its divergence and curl (the well-known Helmholtz theorem [5]). Therefore, the field of the light energy flux is generally vortical in character, the vortical nature of the flux being most pronounced in the vicinity of zeroes of the complex amplitude, which are referred to as optical vortices. It is significant that similarly to the field energy itself, the curl of the light energy flux vector obeys a conservation law: the integral of the curl's projection on the direction of propagation is equal to zero in any plane in the Fresnel zone. As is also shown in Refs [3, 4], it is impossible to find the vortical component from the measurements of the intensity and its derivative and, accordingly, to reconstruct the initial field. At a qualitative level, this can supposedly be explained as follows. In the one-dimensional case, a nonzero phase gradient is always responsible for local intensity changes during propagation (the energy goes either to the right or to the left), but in the two-dimensional case, energy circulation due to the vortical component is possible such that it is not necessarily manifested in the form of a local intensity change. This consideration is also supported by the fact that a two-dimensional field devoid of the vortical component, for instance, a radially symmetric field, can be reconstructed from intensity measurements. The variation in such fields during propagation may in a sense be associated with tensile–compressive deformations (without torsion).

Optical vortices are zeroes of the complex amplitude of the light field, at which the phase distribution has singularities. They are termed wavefront dislocations. Initially, this term was introduced and considered from a geometrical standpoint by J F Nye and M V Berry [6], who called attention to the fundamental difference between the zeroes of the complex amplitude of the wave field in one- and two-dimensional cases. The meaning of this difference is as follows. For a one-dimensional field, the locus of the zeroes of the real and imaginary parts of the complex field amplitude is a set of points, but for a two-dimensional field, the loci of the zeroes of the real and imaginary parts are lines. That is why the behavior of isolated amplitude zeroes becomes different on small variations (stirs) in the field: in the one-dimensional case, the zero points of the real and imaginary parts easily 'lose sight' of each other and the amplitude zero disappears; in the two-dimensional case, the zero lines of the real and imaginary parts are deformed, but the points of their intersection, i.e., the isolated amplitude zeroes, remain stable. The field phase is undefined at the zeroes of its amplitude and has a helical structure in the vicinity of each zero, while the circulation of the phase gradient around them is an integer multiple of 2π. Such isolated points have come to be known as wavefront dislocations, or phase singularities. The sign of a wavefront dislocation is determined by the sign of the phase incursion in going round it.

Of compatriot scientists, B Ya Zel'dovich et al. [7, 8] placed emphasis on these optical objects. They studied the density and sign of dislocations in a random light field (a speckle field). In particular, they showed that the number of dislocations of either sign in the speckle field is approximately equal, while the dislocation density is one dislocation per speckle (i.e., the characteristic average dimension of field irregularity).

Light fields with phase singularities are being investigated by the scientific groups of M S Soskin, A V Volyar, and A Ya Bekshaev. They have investigated the topological properties of these fields [9 – 12], the methods for synthesizing them with the aid of specific holograms [13], the magnitude and structure of the angular momentum of beams with phase singularities [14, 15], and the propagation of vortical beams through few-mode fibers [16]. Of other publications on this subject, we note Refs [17 – 25]. Presently, the area of investigation concerned with such fields is commonly referred to as singular optics. Three international conferences have been organized on this subject [26 – 28].

The nonlinear optics of light fields with wavefront dislocations is an important branch of singular optics in its own right, where the fields, while retaining the vortical character during propagation, typically undergo qualitative changes. In this review, we discuss only those vortical light fields in a linear optical medium that are self-similar in intensity. The nonlinear optics of light beams with phase singularities has a specific character of its own and deserves a special review. We nevertheless consider it necessary to mention Refs [29 – 37] on this subject.

Taking the vortical component of the vector field of light energy flux into account, one can extend the notion of structural stability and investigate the question of the existence of light fields retaining, up to scale and rotation, the form of intensity during propagation. This problem is formulated and investigated in Section 2. Also given in Section 2 is the complete description of such beams, which are termed spiral. Section 3 is concerned with the theoretical and experimental investigation of the feasibility of synthesis of structurally stable rotating fields with a desired intensity distribution. Also shown in Section 3 is the application of the results obtained on the optics of spiral beams to the problem of the synthesis of phase elements that focus the radiation on some flat curve. Considered in Section 4 are the issues related to the angular momentum and other integral invariants of spiral beams.

2. Spiral laser beams

2.1 Light fields rotating during propagation

Let a coherent light field with a wavelength λ be specified by its complex amplitude $F(x, y, l)$. We consider the problem of searching for structurally stable light fields in the paraxial approximation, i.e., under the assumption that during the propagation, the field $F(x, y, l)$ varies along x and y much more weakly than along l. In this case, the l variable is referred to as the propagation variable and the field evolution is described by the parabolic equation [1]

$$\frac{\partial^2 F}{\partial x^2} + \frac{\partial^2 F}{\partial y^2} + 2ik\,\frac{\partial F}{\partial l} = 0\,, \qquad (1)$$

where $k = 2\pi/\lambda$ is the wavenumber. For a helium – neon laser, for instance, $\lambda = 0.63$ μm, and hence $k \sim 10^7$ m^{-1}.

[1] This term does not correspond to the mathematical classification of second-order partial differential equations but is universally accepted in optics [38].

It is well known [38, 39] that the fundamental solution of Eqn (1) is

$$G(x,y,l)=\frac{k}{2\pi \mathrm{i}l}\exp\left[\frac{\mathrm{i}k}{2l}(x^2+y^2)\right],$$

and therefore the solution of the parabolic equation subjected to the initial condition $F(x,y,0)=F_0(x,y)$ is given by

$$F(x,y,l)=\frac{k}{2\pi \mathrm{i}l}\iint_{\mathbf{R}^2}\exp\left\{\frac{\mathrm{i}k}{2l}\left[(x-\xi)^2+(y-\eta)^2\right]\right\}\times F_0(\xi,\eta)\,\mathrm{d}\xi\,\mathrm{d}\eta\,. \tag{2}$$

Here, the integral on the right-hand side is termed the Fresnel transformation of the function $F_0(\xi,\eta)$. The transformation inverse to transformation (2) also bears the name of Fresnel:

$$F_0(\xi,\eta)=-\frac{k}{2\pi \mathrm{i}l}\iint_{\mathbf{R}^2}\exp\left\{-\frac{\mathrm{i}k}{2l}\left[(x-\xi)^2+(y-\eta)^2\right]\right\}\times F(x,y,l)\,\mathrm{d}x\,\mathrm{d}y\,.$$

With the use of Fresnel's integral operator, equality (2) takes the form $F(x,y,l)=\mathbf{FR}_l\left[F_0(\xi,\eta)\right]$ and the inverse transformation becomes $F_0(\xi,\eta)=\mathbf{FR}_{-l}\left[F(x,y,l)\right]$. Both formulas are special cases of a more general equality that relates the complex-valued distributions of the light field F in the planes l_1 and l_2:

$$F(x,y,l_2)=\mathbf{FR}_{l_2-l_1}\left[F(\xi,\eta,l_1)\right]. \tag{3}$$

For functions $F_0(\xi,\eta)\in L_2(\mathbf{R}^2)$, the Parseval equality

$$\iint_{\mathbf{R}^2}\left|F(x,y,l)\right|^2\mathrm{d}x\,\mathrm{d}y=\iint_{\mathbf{R}^2}\left|F_0(\xi,\eta)\right|^2\mathrm{d}\xi\,\mathrm{d}\eta$$

expresses the energy conservation law for light fields: the total energy of a light field is constant and independent of the chosen plane l.

In the subsequent discussion, we use the following terminology: $I(x,y,l)=F(x,y,l)\bar{F}(x,y,l)$ is called the intensity and $\varphi(x,y,l)=\arg F(x,y,l)$ the phase of a function F. (Hereinafter, the bar denotes complex conjugation.) As a consequence, the representation of $F(x,y,l)$ in terms of the intensity and phase is given by

$$F(x,y,l)=\sqrt{I(x,y,l)}\,\exp\left[\mathrm{i}\varphi(x,y,l)\right].$$

The structural stability condition for the intensity of a light field rotating during propagation can be written as

$$I(x,y,l)=D(l)I_0\left(\frac{x\cos\theta(l)-y\sin\theta(l)}{d(l)},\frac{x\sin\theta(l)+y\cos\theta(l)}{d(l)}\right), \tag{4}$$

where $\theta(l)$ is the dependence of the rotation angle of the intensity distribution during propagation of the field $F(x,y,l)$ and $d(l)>0$ is the scaling intensity variation. We define real variables X and Y by the equality

$$X+\mathrm{i}Y=\frac{(x+\mathrm{i}y)\exp\left[\mathrm{i}\theta(l)\right]}{d(l)}\,.$$

Using the variables X, Y, and l instead of x, y, and l, we can write the structural intensity stability condition in the most compact form: the function $I_0(X,Y)$ is independent of l. Applying the energy conservation law allows expressing $D(l)$ in terms of $d(l)$:

$$\iint_{\mathbf{R}^2}I(x,y,l)\,\mathrm{d}x\,\mathrm{d}y=D(l)d^2(l)\iint_{\mathbf{R}^2}I_0(X,Y)\,\mathrm{d}X\,\mathrm{d}Y=\mathrm{const}\,.$$

Consequently, $D(l)=1/d^2(l)$.

Therefore, the problem of searching for structurally stable light fields $F(x,y,l)$ whose intensity may only rotate or vary in scale during propagation also requires finding the functions $d(l)$ and $\theta(l)$ that characterize the behavior of $I(x,y,l)$ with l.

The starting point in the solution of the above problem is rewriting Eqn (1) in the real notation. In terms of the intensity $I(x,y,l)$ and phase $\varphi(x,y,l)$, this equation is equivalent to the system

$$\begin{cases}\dfrac{\partial}{\partial x}\left(I\dfrac{\partial\varphi}{\partial x}\right)+\dfrac{\partial}{\partial y}\left(I\dfrac{\partial\varphi}{\partial y}\right)+k\dfrac{\partial I}{\partial l}=0\,,\\ 2I\left(\dfrac{\partial^2 I}{\partial x^2}+\dfrac{\partial^2 I}{\partial y^2}\right)-\left(\dfrac{\partial I}{\partial x}\right)^2-\left(\dfrac{\partial I}{\partial y}\right)^2\\ \quad -4I^2\left[\left(\dfrac{\partial\varphi}{\partial x}\right)^2+\left(\dfrac{\partial\varphi}{\partial y}\right)^2+2k\dfrac{\partial\varphi}{\partial l}\right]=0\,.\end{cases} \tag{5}$$

We substitute expression (4) for the intensity in the first equation of this system and rewrite it in terms of the variables X, Y, and l,

$$\boldsymbol{\nabla}\left\{I_0\boldsymbol{\nabla}\left[\varphi-\frac{1}{2}\,k\,d(l)d'(l)(X^2+Y^2)\right]\right\}+k\theta'(l)d^2(l)\left(X\frac{\partial I_0}{\partial Y}-Y\frac{\partial I_0}{\partial X}\right)=0\,,$$

where $\boldsymbol{\nabla}=(\partial/\partial X,\partial/\partial Y)$. We then define the function $\varphi_0(X,Y,l)$ by the equality

$$\varphi(x,y,l)=\frac{1}{2}\,k\,d(l)d'(l)(X^2+Y^2)+\varphi_0(X,Y,l)\,,$$

with the result that the structurally stable light field $F(x,y,l)$ assumes the form

$$F(x,y,l)=\frac{1}{d(l)}\sqrt{I_0(X,Y)}\times\exp\left[\frac{1}{2}\,\mathrm{i}k\,d(l)d'(l)(X^2+Y^2)+\mathrm{i}\varphi_0(X,Y,l)\right]. \tag{6}$$

In terms of the variables X, Y, and l and the functions I_0 and φ_0, system (5) then becomes

$$\begin{cases}\boldsymbol{\nabla}(I_0\boldsymbol{\nabla}\varphi_0)+kd^2(l)\theta'(l)\left(X\dfrac{\partial I_0}{\partial Y}-Y\dfrac{\partial I_0}{\partial X}\right)=0\,,\\ |\boldsymbol{\nabla}\varphi_0|^2+k^2d^3(l)d''(l)(X^2+Y^2)+2kd^2(l)\dfrac{\partial\varphi_0}{\partial l}\\ \quad +2kd^2(l)\theta'(l)\left(X\dfrac{\partial\varphi_0}{\partial Y}-Y\dfrac{\partial\varphi_0}{\partial X}\right)\\ \quad -\dfrac{1}{2I_0}\left(\boldsymbol{\nabla}^2I_0-\dfrac{|\boldsymbol{\nabla}I_0|^2}{2I_0}\right)=0\,.\end{cases} \tag{7}$$

The fact that the phase φ_0, unlike the intensity I_0, depends on all the three variables X, Y, and l does not allow simplifying nonlinear system (7) and turns the search for its solutions into

an extremely complicated task. However, under an additional assumption about the asymptotic behavior of the intensity for large $x^2 + y^2$, invoking complex analysis (namely, the results that relate the properties of functions to the properties of their Fourier transforms) enables the solution of the problem to be brought to specific analytic expressions.

2.2 Order of growth and structural form of solutions

The following statement is of significance for the determination of the form of solutions. Let $F(x, y, l)$ be a solution of parabolic equation (1) and let it be structurally stable in the sense specified in (4). For all $(x, y) \in \mathbf{R}^2$, let the intensity on the plane $l = 0$ satisfy the inequality

$$I(x, y, 0) \leqslant C \exp\left[-A\left(|x|^{\alpha} + |y|^{\alpha}\right)\right] \tag{8}$$

for some $A > 0$, $C > 0$, and $\alpha \geqslant 2$. Then, the analytic continuation of $F(x, y, l)$ in the variables x, y is an entire function of the second order of growth[2] and $\alpha = 2$. In particular, there exist no structurally stable light fields whose intensity decreases faster than the Gaussian function.

To prove this, we rewrite the integral Fresnel transformation (3) as follows:

$$F(x, y, l_2) = \frac{k}{2\pi \mathrm{i}(l_2 - l_1)} \exp\left[\frac{\mathrm{i}k(x^2 + y^2)}{2(l_2 - l_1)}\right] \times \iint_{\mathbf{R}^2} \exp\left[-\frac{\mathrm{i}k(x\xi + y\eta)}{l_2 - l_1}\right] \times \exp\left[\frac{\mathrm{i}k(\xi^2 + \eta^2)}{2(l_2 - l_1)}\right] F(\xi, \eta, l_1)\, \mathrm{d}\xi\, \mathrm{d}\eta\,.$$

This allows us to consider the respective functions $F(x, y, l_1)$ and $F(x, y, l_2)$ for arbitrary l_1 and l_2 as the initial field and its Fourier transform with some purely phase factor, and vice versa. As shown in Ref. [42], if $f(z, w)$ is an entire function of two complex variables that satisfies the inequality

$$\left|f(x, y)\right| \leqslant C \exp\left[-A\left(|x|^{\alpha} + |y|^{\alpha}\right)\right] \tag{9}$$

for some $C > 0$, $A > 0$, and $\alpha > 0$ for all $(x, y) \in \mathbf{R}^2$, then $\rho_f \geqslant \alpha$.

Furthermore [43], if $f(x, y)$ is a square-integrable function that satisfies inequality (9) for some $C > 0$, $A > 0$, and $\alpha > 1$, its Fourier transform

$$F(x, y) = \iint_{\mathbf{R}^2} \exp\left[-\mathrm{i}(x\xi + y\eta)\right] f(\xi, \eta)\, \mathrm{d}\xi\, \mathrm{d}\eta$$

is continued to an entire function $F(z, w)$ of two complex variables z, w and the order of growth of this function does not exceed $\alpha/(\alpha - 1)$.

Therefore, the structural stability condition for the solution $F(x, y, l)$ of the parabolic equation implies that the order of growth of $F(x, y, l)$ must simultaneously satisfy the conditions $\alpha \leqslant \rho_F \leqslant \max\left(2, \alpha/(\alpha - 1)\right)$. Because $\alpha \geqslant 2$, it follows that $\alpha/(\alpha - 1) \leqslant 2$ and the field $F(x, y, l)$ is a function of the second order of growth. The strict inequality $\alpha > 2$ leads to the contradiction $2 < \rho_F \leqslant 2$ and thereby prohibits the existence of structurally stable solutions of the parabolic equation whose intensity decreases faster than the Gaussian function.

It is pertinent to note that the question of whether there exist structurally stable fields whose intensity decreases slower than the Gaussian function $\exp\left[-A(x^2 + y^2)\right]$ is still open,[3] and the subsequent discussion is dedicated to structurally stable solutions of the parabolic equation that are described by entire functions of the second order of growth.

It can be shown [45, 46] that if $F(x, y, l)$ is a solution of parabolic equation (1) possessing structural stability and satisfying inequality (8), then the X, Y, and l variables in representation (6) separate and the phase $\varphi_0(X, Y, l)$ assumes the form

$$\varphi_0(X, Y, l) = \varphi_0(X, Y, 0) + \gamma(l)\,, \tag{10}$$

where $\gamma(l)$ is some function.

Therefore, the exponential intensity decrease at infinity allows revealing the structure of the phase $\varphi_0(X, Y, l)$ and makes the form of expression (6) specific,

$$F(x, y, l) = \frac{1}{d(l)}\, F_0(X, Y) \times \exp\left[\frac{1}{2}\, \mathrm{i}kd(l)d'(l)(X^2 + Y^2) + \mathrm{i}\gamma(l)\right], \tag{11}$$

where $F_0(X, Y) = \sqrt{I_0(X, Y)}\, \exp\left[\mathrm{i}\varphi_0(X, Y, 0)\right]$ is an entire function of the second order of growth. The structural stability of the intensity, Eqn (4), therefore implies structural phase stability up to defocusing.

2.3 Basic equations and parameters of solutions

In this section, we find the scaling $d(l)$, rotation $\theta(l)$, and phase incursion $\gamma(l)$ functions and also indicate the way to derive the function $F_0(X, Y)$, which plays the decisive part in representation (11) of structurally stable solutions of the parabolic equation [45].

Using equality (10) in Eqns (7) enables us to determine the l-dependences of d, θ, and γ. It is easily shown that these three functions satisfy the following system of differential equations:

$$d^3(l)\, d''(l) = \mathrm{const}\,,$$
$$d^2(l)\, \theta'(l) = \mathrm{const}\,,$$
$$d^2(l)\, \gamma'(l) = \mathrm{const}\,.$$

The general solution of this system is given by

$$d(l) = d_0 \sqrt{1 + \frac{4(l - l_0)^2}{k^2 \rho^4}}\,,$$

$$\theta(l) = \theta_0 \arctan\left(\frac{2(l - l_0)}{k\rho^2}\right) + \theta_1\,,$$

$$\gamma(l) = -\gamma_0 \arctan\left(\frac{2(l - l_0)}{k\rho^2}\right) + \gamma_1\,,$$

[2] The order of growth ρ_f of an entire function $f(z, w)$ is defined as [40, 41]

$$\rho_f = \varlimsup_{R \to \infty} \frac{\ln \ln \max\limits_{|z| = |w| = R} |f(z, w)|}{\ln R}\,.$$

As a consequence, for any $\varepsilon > 0$, there exist positive constants C_0 and A_0 such that the inequality $|f(z, w)| < C_0 \exp\left[A_0\left(|z|^{\rho_f + \varepsilon} + |w|^{\rho_f + \varepsilon}\right)\right]$ is satisfied for all complex z and w.

[3] More precisely: there exist no structurally stable fields with the order of growth $\rho_F \leqslant 1$, because the Fourier transform of such fields has singularities and is therefore not an entire analytic function [44]. Therefore, the interval $\rho_F \in (1, 2)$ remains unexplored.

where d_0, θ_0, θ_1, γ_0, γ_1, l_0, and ρ are arbitrary constants.[4] Without losing the generality, it may be assumed that $d_0 = 1$ and $l_0 = \theta_1 = \gamma_1 = 0$. Representation (11) then takes the form

$$F(x, y, l) = \frac{1}{|\sigma|} F_0(X, Y) \exp\left[\frac{2il}{k\rho^2}(X^2 + Y^2) - i\gamma_0 \arg\sigma\right], \tag{12}$$

where $X + iY = (x + iy)\exp(i\theta_0 \arg\sigma)/\rho|\sigma|$ and $\sigma = 1 + 2il/k\rho^2$ is a complex parameter introduced for compactness of notation. Upon substitution of expression (12) in Eqn (1), we obtain the equation for the function $F_0(X, Y)$:

$$\nabla^2 F_0 + 4i\theta_0\left(X\frac{\partial F_0}{\partial Y} - Y\frac{\partial F_0}{\partial X}\right) - 4F_0(X^2 + Y^2 - \gamma_0) = 0. \tag{13}$$

For $\theta_0 = 0$, this equation is a stationary Schrödinger equation for a harmonic oscillator and its solutions are well known [48, 49]. These are the Hermite–Gauss functions $F_0(X, Y) = \mathcal{H}_{n,m}(X, Y)$, $\gamma_0 = n + m + 1$ and the Laguerre–Gauss functions $F_0(X, Y) = \mathcal{L}_{n,\pm m}(X, Y)$, $\gamma_0 = 2n + m + 1$. Here,

$$\mathcal{H}_{n,m}(X, Y) \stackrel{\text{def}}{=} \exp(-X^2 - Y^2)\, H_n(\sqrt{2}X)\, H_m(\sqrt{2}Y) \qquad (n, m = 0, 1, \ldots),$$

$$\mathcal{L}_{n,\pm m}(X, Y) \stackrel{\text{def}}{=} \exp(-X^2 - Y^2)(X \pm iY)^m L_n^m(2X^2 + 2Y^2) \qquad (n, m = 0, 1, \ldots),$$

where

$$H_n(t) = (-1)^n e^{t^2}\frac{d^n}{dt^n}(e^{-t^2}),$$

$$L_n^m(t) = \frac{1}{n!}\, t^{-m} e^t \frac{d^n}{dt^n}(t^{n+m} e^{-t})$$

are the Hermite and Laguerre polynomials, respectively.

We seek the solutions of Eqn (13) in the form of the expansion

$$F_0(X, Y) = \sum_{n=0}^{\infty}\sum_{m=-\infty}^{\infty} c_{nm}\mathcal{L}_{n,m}(X, Y), \tag{14}$$

which is always possible owing to inequality (8) and the completeness of the system of functions $\{\mathcal{L}_{n,m}(X, Y),\ n, \pm m = 0, 1, \ldots\}$ in the space $L_2(\mathbf{R}^2)$. We substitute expansion (14) in Eqn (13) to obtain the identity

$$\sum_{n,m} c_{nm}\mathcal{L}_{n,m}(X, Y)(2n + |m| + \theta_0 m - \gamma_0 + 1) = 0$$

or, in view of the completeness of the system of Laguerre–Gauss functions, an infinite set of constraints on the coefficients c_{nm} and the numbers n, m:

$$c_{nm}(2n + |m| + \theta_0 m - \gamma_0 + 1) = 0.$$

Once some pair (n_0, m_0) is fixed, the problem of searching for $F_0(X, Y)$ reduces to determining the integers n and m from the equation

$$2n + |m| + \theta_0 m = 2n_0 + |m_0| + \theta_0 m_0. \tag{15}$$

In this formula, n and n_0 are nonnegative integers, m and m_0 are integers, and θ_0 is a real number. We then have $\gamma_0 = 2n_0 + |m_0| + \theta_0 m_0 + 1$ and the coefficients c_{nm} are arbitrarily selected for those pairs (n, m) that satisfy Eqn (15) and are equal to zero otherwise.

We next show that Eqn (15) is solvable for any θ_0 and find the corresponding solutions of Eqn (13).

2.4 Spiral beams and their quantum-mechanical analogs

We let $\mathcal{N}(\theta_0)$ denote the ensemble of all pairs (n, m) satisfying Eqn (15). The complete specification of the ensemble $\mathcal{N}(\theta_0)$ for different θ_0 and the definition of the functions $F_0(X, Y)$ reduce to the following three cases.

1. If θ_0 is an irrational number, the ensemble $\mathcal{N}(\theta_0)$ consists of a single pair (n_0, m_0). By invoking the definition of Laguerre–Gauss functions, it is easily shown that the structurally stable field $F(x, y, l)$ is independent of θ_0 and can be represented as

$$F(x, y, l) = \frac{1}{|\sigma|}\exp\left[\frac{2il(x^2 + y^2)}{k\rho^4|\sigma|^2} - i(2n_0 + |m_0| + 1)\arg\sigma\right] \times \mathcal{L}_{n_0, m_0}\left(\frac{x}{\rho|\sigma|}, \frac{y}{\rho|\sigma|}\right). \tag{16}$$

Obviously, the absence of the θ_0-dependence is the underside of the radially symmetric form of field intensity (16), because it makes no difference in this case what rotation to assign to this field.

2. If $\theta_0 = 0$, then $\theta(l) \equiv 0$ and the corresponding field $F(x, y, l)$ propagates along l without rotation. In this case, $\mathcal{N}(0) = \{(n, m);\ 2n + |m| = N\}$, where $N = 0, 1, \ldots$, $\gamma_0 = N + 1$, and

$$F(x, y, l) = \frac{1}{|\sigma|}\exp\left[\frac{2il(x^2 + y^2)}{k\rho^4|\sigma|^2} - i(N + 1)\arg\sigma\right] \times \sum_{n=0}^{N} c_n \mathcal{L}_{\min(n, N-n),\, N-2n}\left(\frac{x}{\rho|\sigma|}, \frac{y}{\rho|\sigma|}\right), \tag{17}$$

where c_n are arbitrary constants. The resultant expression shows that in the paraxial approximation only the fields whose beam waist is given by a Gaussian function times some polynomial of a special form can propagate with retention of their structure and without rotation. Moreover,

$$|F(x, y, l)| = |F(-x, -y, l)|,$$

i.e., the intensity of any nonrotating structurally stable field has central symmetry. Such fields are exemplified in Fig. 1. The Hermite–Gauss mode depicted in Fig. 1a is a real function, and its phase therefore assumes only the 0 and π values. The horizontal and vertical straight lines in the phase distribution of the Hermite–Gauss mode show the location of zero lines: in crossing such a line, there occurs a phase jump by π. The Laguerre–Gauss modes have both zero lines (circles) and an isolated zero at the origin.

Isolated zeroes (points of phase singularity) are conveniently classified by the magnitude of the shift acquired by the phase in going round such a zero counterclockwise. If the phase incursion is positive, the zero is termed a z-type zero, and if the incursion is negative, a $\bar{z}$-type zero. Although this

[4] The special case $\rho = \infty$ corresponds to nondiffracting beams [47], for instance, Bessel beams, $F(x, y, l) = J_m(\sqrt{2k\gamma_0}\, r)\exp(im\alpha - i\gamma_0 l)$, where r and α are polar coordinates. Such beams do not have finite energy and are not considered in our review.

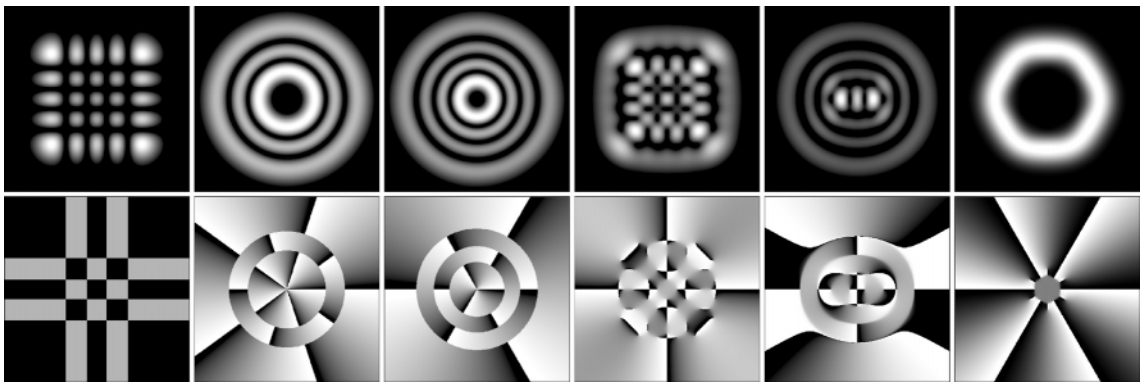

Figure 1. Intensities (upper row) and phases (lower row) of structurally stable fields without rotation: (a) the Hermite – Gauss mode $\mathscr{H}_{4,4}(x,y)$; (b, c) Laguerre – Gauss modes $\mathscr{L}_{2,5}(x,y)$ and $\mathscr{L}_{3,-3}(x,y)$; (d, e) Hermite – Laguerre – Gauss modes $\mathscr{G}_{4,4}(x,y|\pi/10)$ and $\mathscr{G}_{5,3}(x,y|\pi/5)$ (see Ref. [50]); (f) the field of form (17) for $N=8$ with a special set of coefficients c_n to make its intensity look like a regular hexagon. In all drawings, black color corresponds to the zero intensity and zero phase, white color corresponds to the maximum intensity and the phase 2π.

classification does not reflect the entire diversity of possibilities (the zero lines of the real and imaginary parts of the complex amplitude do not necessarily intersect at a right angle and may be quite different in form from linear functions even in a small neighborhood of the zero), it furnishes the simplest characteristic of phase behavior in the vicinity of each isolated zero.

The phase singularity point for the $\mathscr{L}_{2,5}(x,y)$ mode is a z-type zero of the fifth order: in going round it counterclockwise, the phase changes five times from 0 to 2π. For the $\mathscr{L}_{3,-3}(x,y)$ mode, a similar point at the origin is an isolated $\bar{z}$-type zero of the third order. The structurally stable fields shown in Figs 1d – f have isolated zeroes of the z-type, as well as the $\bar{z}$-type. Contrasting black – white changes in the phase distributions correspond to splices of the $\varphi=0$ and $\varphi=2\pi$ phases.

3. Let $\theta_0=-1$. Then, $2n+|m|-m$ is an even nonnegative number. Setting it equal to $2N$, we find the ensemble

$$\mathscr{N}(-1)=\{(N,m);m=0,1,2,\dots\}\cup\{(N+m,m);m=-1,-2,\dots,-N\},$$

the phase incursion parameter $\gamma_0=2N+1$, and the light field

$$F(x,y,l)=\frac{1}{|\sigma|}\exp\left[\frac{2\mathrm{i}l(x^2+y^2)}{k\rho^4|\sigma|^2}-\mathrm{i}(2N+1)\arg\sigma\right]\times\left[\sum_{m=0}^{\infty}c_m\mathscr{L}_{N,m}(X,Y)+\sum_{m=1}^{N}c_{-m}\mathscr{L}_{N-m,-m}(X,Y)\right], \quad (18)$$

where $X+\mathrm{i}Y=(x+\mathrm{i}y)/\rho\sigma$. For $N=0$, the simple form of the Laguerre – Gauss functions

$$\mathscr{L}_{0,m}(X,Y)=\exp(-X^2-Y^2)(X+\mathrm{i}Y)^m$$

allows representing the solution in a more compact form:

$$F(x,y,l)=\frac{1}{\sigma}\exp\left[\frac{2\mathrm{i}l(x^2+y^2)}{k\rho^4|\sigma|^2}\right]\times\sum_{m=0}^{\infty}c_m\exp(-X^2-Y^2)(X+\mathrm{i}Y)^m=\frac{1}{\sigma}\exp\left(-\frac{x^2+y^2}{\rho^2\sigma}\right)f\left(\frac{x+\mathrm{i}y}{\rho\sigma}\right). \quad (19)$$

Here, $f(z)$ is an entire analytic function such that $F(x,y,0)\in L_2(\mathbf{R}^2)$. In view of the formula

$$\theta(l)=-\arctan\left(\frac{2l}{k\rho^2}\right),$$

the evolution of the field intensity $F(x,y,l)$ during propagation looks like a decelerating rotation — the fastest in the beam waist region and nearly zero in the far-field zone. In this case, the total field rotation angle during propagation is $\theta(\infty)-\theta(0)=-\pi/2$.

The general expression (18) can also be given a clearer form using the differential representation of the Laguerre – Gauss functions from Ref. [51]:

$$\mathscr{L}_{n,\pm m}(X,Y)=\frac{(-1)^{n+m}}{2^{n+m}n!}\exp(X^2+Y^2)\times\frac{\partial^n}{\partial(X\pm\mathrm{i}Y)^n}\frac{\partial^{n+m}}{\partial(X\mp\mathrm{i}Y)^{n+m}}\exp(-2X^2-2Y^2).$$

Finally, we have

$$F(x,y,l)=\frac{1}{|\sigma|}\exp\left[\frac{2\mathrm{i}l(x^2+y^2)}{k\rho^4|\sigma|^2}-\mathrm{i}(2N+1)\arg\sigma\right]\times\exp(Z\bar{Z})\frac{\partial^N}{\partial Z^N}\left[\exp(-2Z\bar{Z})f(Z)\right]=\frac{1}{\sigma}\exp\left(-\frac{x^2+y^2}{\rho^2\sigma}-2\mathrm{i}N\arg\sigma\right)\left(\frac{\partial}{\partial Z}-2\bar{Z}\right)^N f(Z), \quad (20)$$

where $Z=(x+\mathrm{i}y)/\rho\sigma$ and $\bar{Z}=(x-\mathrm{i}y)/\rho\bar{\sigma}$.

4. The $\theta_0=1$ case is completely similar to the previous one. We set $2n+|m|+m=2N$ to find

$$\mathscr{N}(1)=\{(N,m);m=0,-1,-2,\dots\}\cup\{(N-m,m);m=1,2,\dots,N\},$$

$\gamma_0=2N+1$, and

$$F(x,y,l)=\frac{1}{|\sigma|}\exp\left[-\frac{x^2+y^2}{\rho^2\sigma}-\mathrm{i}(2N+1)\arg\sigma\right]\times\left(\frac{\partial}{\partial\bar{Z}}-2Z\right)^N f(\bar{Z}), \quad (21)$$

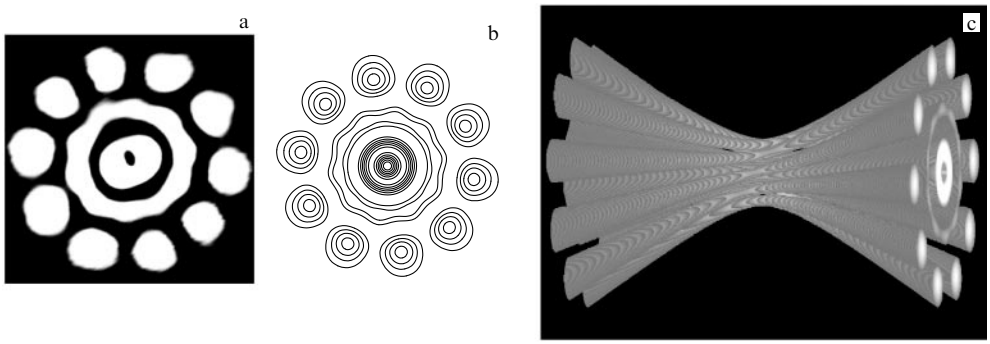

Figure 2. Spiral beam corresponding to the rotation parameter $\theta_0 = -2/5$: (a) experimentally recorded intensity distribution of a spiral beam; (b) level lines for the function $|\mathscr{L}_{0,9}(x,y) - 49\mathrm{i}\mathscr{L}_{2,-1}(x,y)|^2$; (c) fragment of spatial beam propagation in the waist region.

where $Z = (x + \mathrm{i}y)/\rho\bar{\sigma}$ and $\bar{Z} = (x - \mathrm{i}y)/\rho\sigma$. In particular, for $N = 0$, we obtain

$$F(x,y,l) = \frac{1}{\sigma}\exp\left(-\frac{x^2+y^2}{\rho^2\sigma}\right) f\left(\frac{x-\mathrm{i}y}{\rho\sigma}\right). \tag{22}$$

Here, as in expression (19), $f(z)$ is an arbitrary entire function that does not destroy the square integrability of the function $F(x,y,0)$. This condition is fulfilled, for instance, for any entire function $f(z)$ with the order of growth $\rho_f < 2$. In particular, some polynomial can be selected as $f(z)$. Structurally stable fields in this case were simultaneously and independently obtained in Ref. [52].

5. Lastly, if θ_0 is a rational number different from 0 and ± 1, the set $\mathscr{N}(\theta_0)$ contains, along with the pair (n_0, m_0), some pair $(n_1, m_1 \neq m_0)$. In this case,

$$\theta_0 = \frac{2n_0 + |m_0| - 2n_1 - |m_1|}{m_1 - m_0},$$

and the structurally stable solution is given by

$$F(x,y,l) = \frac{1}{|\sigma|}\exp\left[\frac{2\mathrm{i}l(x^2+y^2)}{k\rho^4|\sigma|^2} - \mathrm{i}(2n_0 + |m_0| + \theta_0 m_0 + 1)\arg\sigma\right] \sum_{\mathscr{N}(\theta_0)} c_{nm}\mathscr{L}_{n,m}(X,Y), \tag{23}$$

where $X + \mathrm{i}Y = (x + \mathrm{i}y)\exp(\mathrm{i}\theta_0 \arg\sigma)/\rho|\sigma|$, and the set $\mathscr{N}(\theta_0)$ of all pairs (n,m) over which the summation ranges is determined as follows. We assume that $\operatorname{sgn} m_0 = 1$ for $m_0 \geqslant 0$ and $\operatorname{sgn} m_0 = -1$ for $m_0 < 0$. We represent θ_0 as a fraction P/Q, where P and Q are coprime numbers and $Q > 0$. The following cases can occur: (i) one of the numbers P, Q is even, (ii) both numbers P and Q are odd. In the first case,

$$\mathscr{N}(\theta_0) = \big\{\big(n_0 + (P + Q\operatorname{sgn} m_0)k,\ m_0 - 2Qk\big);\ k \in \mathbf{Z},\ n \geqslant 0,\ m\operatorname{sgn} m_0 \geqslant 0\big\} \cup \big\{\big(n_0 + |m_0| + (P - Q\operatorname{sgn} m_0)k,\ m_0 - 2Qk\big);\ k \in \mathbf{Z},\ n \geqslant 0,\ m\operatorname{sgn} m_0 < 0\big\};$$

in the second case,

$$\mathscr{N}(\theta_0) = \left\{\left(n_0 + \frac{1}{2}(P + Q\operatorname{sgn} m_0)k,\ m_0 - Qk\right);\ k \in \mathbf{Z},\ n \geqslant 0,\ m\operatorname{sgn} m_0 \geqslant 0\right\} \cup \left\{\left(n_0 + |m_0| + \frac{1}{2}(P - Q\operatorname{sgn} m_0)k,\ m_0 - Qk\right);\ k \in \mathbf{Z},\ n \geqslant 0,\ m\operatorname{sgn} m_0 < 0\right\}.$$

The use of these formulas is illustrated by two examples.

Let $\theta_0 = -0.4 = -2/5$. Then, $P = -2$, $Q = 5$, and the set $\mathscr{N}(\theta_0)$ is constructed according to case (i). Selecting the initial pair (n_0, m_0) such that $m_0 > 0$ yields

$$\mathscr{N}\left(-\frac{2}{5}\right) = \left\{(n_0 + 3k, m_0 - 10k),\ k \in \mathbf{Z},\ -\frac{n_0}{3} \leqslant k \leqslant \frac{m_0}{10}\right\} \cup \left\{(n_0 + m_0 - 7k, m_0 - 10k),\ k \in \mathbf{Z},\ \frac{m_0}{10} < k \leqslant \frac{n_0 + m_0}{7}\right\}.$$

In particular, for $n_0 = 0$ and $m_0 = 9$, we obtain $\mathscr{N}(-2/5) = \{(0,9), (2,-1)\}$ and

$$F(x,y,l) = \frac{1}{|\sigma|}\exp\left(-\frac{x^2+y^2}{\rho^2\sigma} - 6.4\mathrm{i}\arg\sigma\right) \times \left[c_1\left(\frac{x+\mathrm{i}y}{\rho|\sigma|}\exp(-0.4\mathrm{i}\arg\sigma)\right)^9 + c_2\frac{x-\mathrm{i}y}{\rho|\sigma|}\exp(0.4\mathrm{i}\arg\sigma)\,L_2^1\left(\frac{2x^2+2y^2}{\rho^2|\sigma|^2}\right)\right].$$

Here, c_1 and c_2 are arbitrary complex constants and $\sigma = 1 + 2\mathrm{i}l/k\rho^2$. A spiral beam corresponding to the values $c_1 = 1$ and $c_2 = -49\mathrm{i}$ is shown in Fig. 2. During its propagation from the beam waist region to the far-field region, the beam rotates by the angle $\theta(\infty) - \theta(0) = \pi\theta_0/2 = -2\pi/10$. The intensity does not change during this rotation, and this beam therefore exemplifies a field invariant under a two-dimensional Fourier transformation.

We now assume that $\theta_0 = -3$. Then, $P = -3$, $Q = 1$, and case (ii) is used to construct $\mathscr{N}(\theta_0)$. Selecting the initial pair $n_0 = m_0 = 0$ gives the set $\mathscr{N}(-3) = \{(k,k),\ k = 0,1,2,\ldots\}$,

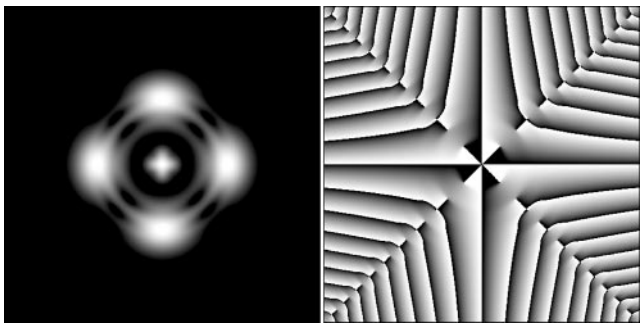

a b

Figure 3. Intensity (a) and phase (b) of the spiral beam corresponding to the rotation parameter $\theta_0 = -3$.

and the spiral beam is

$$F(x,y,l) = \frac{1}{\sigma}\exp\left(-\frac{x^2+y^2}{\rho^2\sigma}\right) \times \sum_{k=0}^{\infty} c_k \left(\frac{x+\mathrm{i}y}{\rho|\sigma|}\exp\left(-3\mathrm{i}\arg\sigma\right)\right)^k L_k^k\left(\frac{2x^2+2y^2}{\rho^2|\sigma|^2}\right).$$

In this case, unlike in the previous one, there are an infinite number of the degrees of freedom, i.e., of the constants c_k involved in constructing the field F. Accordingly, the number of phase singularities in such a beam may be infinite. An example of this kind is provided by a spiral beam constructed on the basis of the modified Bessel function with the following form in its waist plane:

$$F(x,y,0) = \exp\left(-z\bar{z} + az\right)\frac{I_v(2z\sqrt{a^2-2a\bar{z}})}{(2z\sqrt{a^2-2a\bar{z}})^v}.$$

Here, a and v are arbitrary parameters, $z = (x+\mathrm{i}y)/\rho$ and $\bar{z} = (x-\mathrm{i}y)/\rho$ are complex variables. Figure 3 shows the beam $F(x,y,0) + F(y,-x,0) + F(-x,-y,0) + F(-y,x,0)$ for $a = 1.3$ and $v = 1$.

Therefore, we have completed the description of structurally stable solutions of the parabolic equation that satisfy structural representation (4) and inequality (8). The light fields corresponding to solutions (16)–(23) obtained above rotate in accordance with the law $\theta(l) = \theta_0 \arctan(2l/k\rho^2)$ and increase in scale in accordance with the law $d(l) = \sqrt{1+4l^2/k^2\rho^4}$ during their propagation.

We fix some point (x_0, y_0) in the initial plane $l = 0$. During the propagation of the field $F(x,y,l)$, this point traces a spiral path $x+\mathrm{i}y = (x_0+\mathrm{i}y_0)|\sigma|\exp(-\mathrm{i}\theta_0\arg\sigma)$. For small $|\theta_0|$, the term 'spiral' is somewhat conventional and indicates only a tendency toward rotation, but for large $|\theta_0|$, the point (x_0, y_0) executes, during the propagation of the field F, $|\theta_0|/4$ rotations about the l-axis in the clockwise or counterclockwise direction, depending on the sign of θ_0 (Fig. 4). This nonuniform rotation is completed by an asymptotic approach to the straight line

$$x+\mathrm{i}y = (x_0+\mathrm{i}y_0)\left(1+\frac{2\mathrm{i}l}{k\rho^2}\right)\exp\left[-\frac{\pi\mathrm{i}(\theta_0+1)}{2}\right].$$

We also note that the isophase contours of the above solutions are helical outside of the beam waist. These two circumstances have allowed proposing the name 'spiral light beams' for the light fields obtained [45].

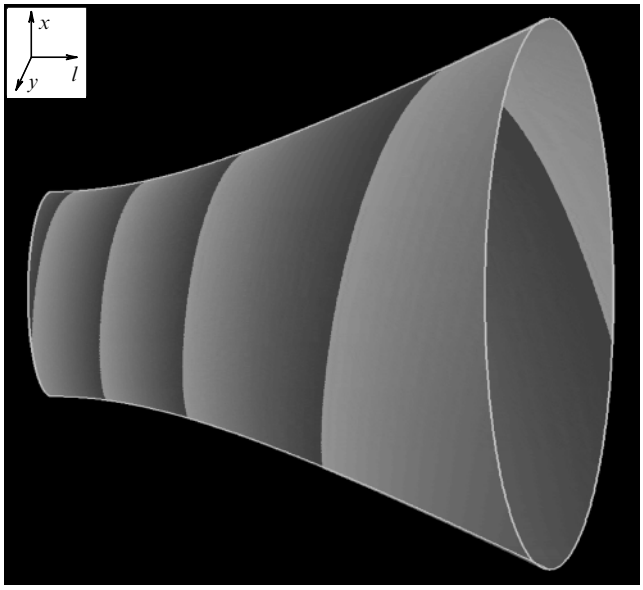

Figure 4. Motion path of a point (x_0, y_0) during the propagation of a spiral beam $F(x,y,l)$ with $\theta_0 = -15$.

The interrelation between paraxial optics and quantum mechanics was considered by several authors (see, e.g., Refs [48, 53]). What specific quantum-mechanical situation corresponds to spiral beams? The equation for spiral beams (13) can be represented in terms of normalized polar coordinates:

$$\nabla^2 F + 4\mathrm{i}\theta_0\frac{\partial F}{\partial\phi} - 4F(R^2-\gamma_0) = 0.$$

Here, R and ϕ are determined from the relation $R\exp(\mathrm{i}\phi) = (x+\mathrm{i}y)\exp(\mathrm{i}\theta_0\arg\sigma)/\rho|\sigma|$.

At the same time, in the standard polar coordinates R and ϕ, the Schrödinger equation for the wave function ψ of a charged particle of mass M and charge e embedded in a uniform magnetic field with an intensity H is written as [54]

$$\nabla^2\psi + 4\mathrm{i}\,\mathrm{sgn}(eH)\frac{\partial\psi}{\partial\phi} - 4\psi\left(R^2 - \frac{2cME_1}{\hbar|eH|}\right) = 0,$$

where $E_1 = E - p_z^2/2M$, E is the particle energy, and p_z is the particle momentum along the field direction. One can see that these equations are equivalent for $\theta_0 = \mathrm{sgn}(eH)$ and $\gamma_0 = 2cME_1/\hbar|eH|$. Therefore, for $\theta_0 = \pm 1$ and $\gamma_0 = 1$, the wave functions of a particle in a constant magnetic field with the ground state $E_1 = \hbar|eH|/2cM$ correspond to spiral beams. It is noteworthy that the form of the above differential equations is the same in different coordinate systems.

2.5 Experimental realization of spiral beams

2.5.1 Astigmatic transformation technique. It is well known [55] that the oscillation frequencies of a stable two-mirror resonator are defined by the expression

$$\omega_q = \frac{2c}{L_0}\left(\gamma\arccos\sqrt{g_1g_2} + \pi q\right), \qquad (24)$$

where c is the speed of light, L_0 is the resonator round-trip time, $g_{1,2} = (1 - L_0/2R_{1,2})$ are configuration parameters,

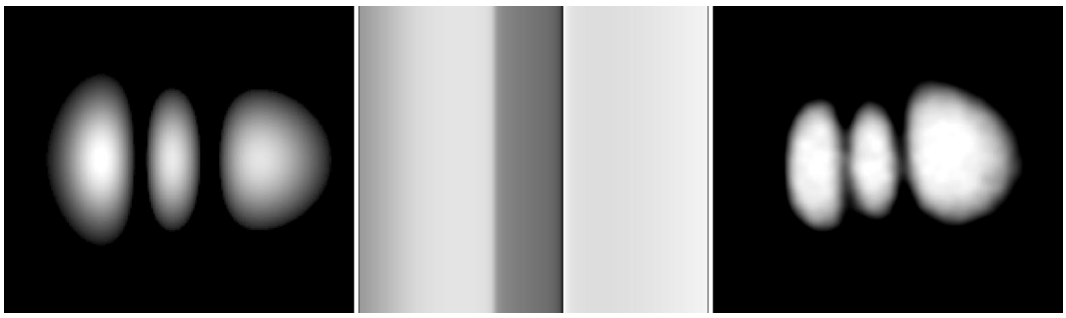

a b c

Figure 5. Intensity (a) and phase (b) of the coding field $\exp(-\rho^2 x^2/8)\, h(y|\triangle_2)$ and experimental intensity distribution (c) of the beam emanating from a helium–neon laser. (The definition of a coding field is given in Section 3.3.)

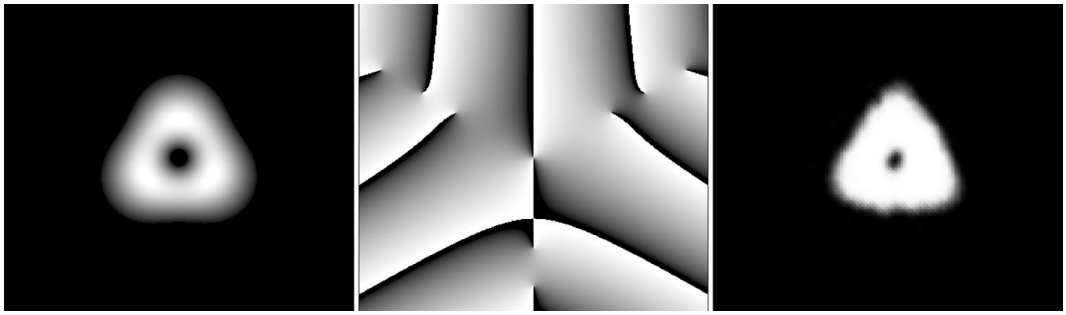

a b c

Figure 6. Intensity (a) and phase (b) of the spiral beam $\mathscr{S}(z, \bar{z}|\triangle_2)$ and its experimental realization (c). The intensity distribution (c) was obtained by astigmatic transformation of the beam whose intensity is shown in Fig. 5c.

$R_{1,2}$ are the curvature radii of the mirrors, q is the axial index, and γ is a parameter equal to $\gamma = n + m + 1$ for the Hermite–Gauss modes $\mathscr{H}_{n,m}(x, y)$ and to $\gamma = 2n + |m| + 1$ for the Laguerre–Gauss modes $\mathscr{L}_{n,m}(x, y)$. It is easily seen that the modes for which $\gamma = \text{const}$ are frequency-degenerate. If the resonator is such that $\arccos\sqrt{g_1 g_2} = \pi M/N$, where M and N are coprime numbers, the frequency degeneracy condition turns out to be also valid for the modes satisfying the condition

$$\gamma M + qN = \text{const}\,. \tag{25}$$

That is why a sum of such modes shows no beats and is also a stationary distribution, which is time-independent at each of its sections. However, it is easy to see that the parameters γ of the terms in the sum are different, and the intensity distribution of such a superposition therefore changes during propagation. For instance, let the generated field be the sum of Laguerre–Gauss modes $\mathscr{L}_{n_1,m_1}(x, y)$ and $\mathscr{L}_{n_2,m_2}(x, y)$ such that $\gamma_1 \neq \gamma_2$ and let constraint (25) be fulfilled. Then, according to solution (23), this sum is a spiral beam with the rotation parameter $\theta_0 = (\gamma_1 - \gamma_2)/(m_2 - m_1)$. In real resonators, however, owing to the presence of astigmatism (for instance, the astigmatism of Brewster windows), Hermite–Gauss modes are ordinarily generated, unless special precautions are taken. That is why it is rather difficult to directly obtain a spiral beam. This situation can be rectified if advantage is taken of the results in Ref. [56], where it was theoretically and experimentally shown that any Hermite–Gauss beam can be transformed into the corresponding Laguerre–Gauss beam and vice versa with the aid of astigmatic optics. The transformation is of the following form:

$$\begin{aligned}
&\iint_{\mathbf{R}^2} \exp\left[-\mathrm{i}(x\xi + y\eta) + \frac{2\mathrm{i}\xi\eta}{\rho^2}\right] \mathscr{H}_{n,m}\left(\frac{\xi}{\rho}, \frac{\eta}{\rho}\right) \mathrm{d}\xi\, \mathrm{d}\eta \\
&\quad = \frac{\pi\rho^2}{\sqrt{2}} (-1)^{n+m} \exp\left(-\frac{\mathrm{i}\rho^2 xy}{4}\right) \\
&\quad \times \begin{cases} (2\mathrm{i})^n m!\, \mathscr{L}_{m,n-m}\left(\dfrac{\rho x}{2\sqrt{2}}, \dfrac{\rho y}{2\sqrt{2}}\right) & (n \geqslant m)\,, \\ (2\mathrm{i})^m n!\, \mathscr{L}_{n,m-n}\left(\dfrac{\rho y}{2\sqrt{2}}, \dfrac{\rho x}{2\sqrt{2}}\right) & (n \leqslant m)\,. \end{cases}
\end{aligned} \tag{26}$$

It can be realized in different ways by means of cylindrical and spherical optics. Examples of the optical schemes and the results of experiments in the specific implementations of transformation (26), which are referred to as astigmatic in what follows, are given in Refs [45, 56].

Let a laser-generated beam be the sum of two Hermite–Gauss modes with the indices (n_1, m_1) and (n_2, m_2), and let $n_1 + m_1 \neq n_2 + m_2$. An astigmatic transformation allows the beam to be transformed into the sum of two Laguerre–Gauss modes with the indices $(\min(n_j, m_j),\ n_j - m_j)$, $j = 1, 2$. The result is a spiral beam with the rotation parameter $\theta_0 = (n_1 + m_1 - n_2 - m_2)/(n_2 + m_1 - n_1 - m_2)$.

As an example, we consider the case where $M/N = 1/3$ (resonator: $R_1 = 2$ m, $R_2 = \infty$, $L_0 = 3$ m). Frequency-degenerate in it is, for instance, the sum of Hermite–Gauss modes of the form $\sum_k c_k \mathscr{H}_{0.3k+2}(x, y)$ (Fig. 5). Such a combination can be realized by introducing thin (15 μm) wires into the resonator field. It is easily seen that a spiral beam with a $2\pi/3$ symmetry is the result of the astigmatic transformation of this field (Fig. 6).

2.5.2 Intracavity synthesis of spiral beams. To determine the resonator configurations allowing a direct generation of spiral beams, we consider the behavior of such a beam in a stable resonator described by the round-trip matrix $ABCD$.

As shown in Section 2.4, an arbitrary spiral beam F with a rotation parameter θ_0 is expressed in terms of Laguerre–Gauss modes at a distance l from the beam waist as

$$F(r,\phi) = \frac{w_0}{w}\exp\left(\frac{\mathrm{i}kr^2}{2R} - \mathrm{i}\gamma_0\Phi_0\right)\sum_{\mathcal{N}(\theta_0)} c_{nm}\mathscr{L}_{n,m}\left(\frac{r}{w},\phi\right)$$
$$= \frac{w_0}{w}\exp\left(\frac{\mathrm{i}kr^2}{2Q} - \mathrm{i}\gamma_0\Phi_0\right)\sum_{\mathcal{N}(\theta_0)} c_{nm}\left(\frac{r}{w}\right)^{|m|}$$
$$\times \exp(\mathrm{i}m\phi)\, L_n^{|m|}\left(\frac{2r^2}{w^2}\right), \qquad (27)$$

where $\mathscr{L}_{n,m}(r,\phi) = \exp(-r^2)r^{|m|}\exp(\mathrm{i}m\phi)\,L_n^{|m|}(2r^2)$ is a Laguerre–Gauss mode in polar coordinates; Φ_0 is the zero-mode phase incursion from the waist plane; w_0 and w are the Gaussian parameters of the beam taken respectively in the waist plane and at the distance l from the plane; $1/Q = 1/R + 2\mathrm{i}/kw^2$ is the complex beam parameter; k is the wavenumber; and $\mathcal{N}(\theta_0)$ is the set of integer-valued pairs (n,m) such that $2n + |m| + \theta_0 m + 1 = \gamma_0 = \text{const}$.

Hereinafter in this section, in lieu of ρ, $\rho|\sigma|$, and $\arg\sigma$, we use the respective variables w_0, w, and Φ_0, because calculations involving the $ABCD$ matrix are commonly described in this notation. Moreover, a polar coordinate system is employed instead of the Cartesian one, making it possible to represent the dependences related to rotation angles more clearly.

After the transformation by an optical system with the $ABCD$ matrix, field (27) becomes [57]

$$F_1(r,\phi) = \frac{w}{w_1}\exp\left(\mathrm{i}kL_0 + \frac{\mathrm{i}kr^2}{2Q_1}\right)$$
$$\times \sum_{\mathcal{N}(\theta_0)} c_{nm}\exp\left[-\mathrm{i}\left(2n + |m| + 1\right)\Phi\right]\left(\frac{r}{w_1}\right)^{|m|}$$
$$\times \exp(\mathrm{i}m\phi)\, L_n^{|m|}\left(\frac{2r^2}{w_1^2}\right), \qquad (28)$$

where L_0 is the optical path length along the axis of the system, $w_1^2 = w^2|A + B/Q|^2$, $\Phi = \arg(A + B/Q)$, $Q_1 = (AQ + B)/(CQ + D)$, and $AD - BC = 1$. Now let $ABCD$ be the round-trip matrix of some stable resonator. From the condition for the self-reproduction of each term of field (27) in the resonator round trip, $Q_1 = Q$, we obtain

$$w_1 = w, \quad \frac{kw^2}{2} = \frac{B}{\sqrt{1 - (A+D)^2/4}}, \quad \Phi = \arccos\frac{A+D}{2}.$$

Then, in view of the relation $2n + |m| + 1 = \gamma_0 - \theta_0 m$, the evolution of spiral beam (27) in tracing the resonator is as follows:

$$F_1(r,\phi) = \exp\left(\mathrm{i}kL_0 - \mathrm{i}\gamma_0\arccos\frac{A+D}{2}\right)$$
$$\times F\left(r, \phi + \theta_0\arccos\frac{A+D}{2}\right). \qquad (29)$$

Here, L_0 is the resonator round-trip path length. It is evident from expression (29) that upon tracing the resonator, the beam rotates by the angle

$$\theta_N = \theta_0\arccos\frac{A+D}{2}$$

and acquires the phase shift

$$\phi_N = kL_0 - \gamma_0\arccos\frac{A+D}{2}.$$

Hence, it is clear that it suffices to effect the beam rotation by the angle $-\theta_N$, or by the angle $2\pi - \theta_N$ for its self-reproduction condition to be fulfilled. It is well known that such rotations are accomplishable in ring resonators, for instance, with the aid of a Dove prism (the so-called resonators with field rotation) [55]. Resonators of this type were employed to improve the uniformity of the transverse laser radiation distribution. However, in contrast to our work, the angle of beam rotation in the above-mentioned resonators was selected irrespective of the resonator configuration parameters (commonly $\pi/2$ or π). If this resonator effects a field rotation by an angle $-\theta_N$ or $2\pi - \theta_N$ and the equality

$$kL_0 - \gamma_0\arccos\frac{A+D}{2} = 2\pi q$$

holds, the condition for beam self-reproduction $F_1(r,\phi) = F(r,\phi)$ is fulfilled and field (27) is the eigenmode of this resonator with the oscillation frequency

$$\omega_q = \frac{c}{L_0}\left(\gamma_0\arccos\frac{A+D}{2} + 2\pi q\right). \qquad (30)$$

It follows that in contrast to an ordinary resonator without beam rotation ($\theta_0 = 0$), the Laguerre–Gauss modes satisfying the condition $2n + |m| + \theta_0 m = \text{const}$ are frequency-degenerate and the degeneracy condition depends on the angle of beam rotation in the resonator. This is easily understood by noting that the rotation of the complex amplitude distribution of the Laguerre–Gauss beam $\mathscr{L}_{n,m}(r,\phi)$ by an angle θ is equivalent to the additional phase shift $m\theta$:

$$\mathscr{L}_{n,m}(r,\phi+\theta) = \mathscr{L}_{n,m}(r,\phi)\exp(\mathrm{i}m\theta).$$

Figure 7 shows a setup assembled for the experimental testing of intracavity synthesis of spiral beams. The ring laser was made on the basis of an argon-ion laser with the wavelength $\lambda = 0.488$ μm, a plane mirror M_1 (with the reflectivity 0.94) and spherical mirrors M_2, M_3 ($R_2 = R_3 = R = 3$ m, with the respective reflectivities 0.995 and 0.98). The mirror separations were $M_1M_2 = M_1M_3 = l = 1.27$ m and $M_2M_3 = l_0 = 2.4$ m. The resonator geometry in the form of an obtuse-angle triangle was selected to reduce the effect of astigmatism of mirrors M_2 and M_3. The field rotation is effected with the aid of a Dove prism P (rotating

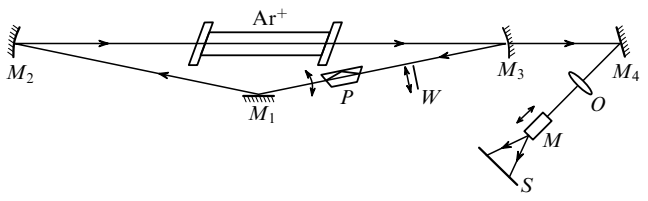

Figure 7. Experimental ring-laser setup involving an argon-ion laser.

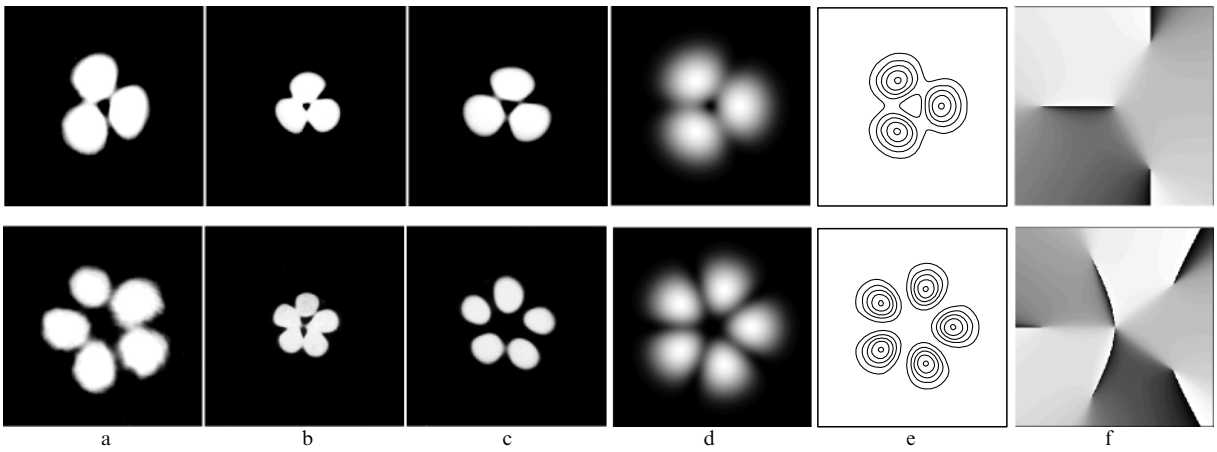

Figure 8. Experimentally recorded intensities of spiral beams in front of (a), inside (b), and behind (c) the waist region for a prism rotation angle α. Theoretical intensity (d) and phase (f) distributions, as well as intensity level lines (e) of a spiral beam with a rotation parameter θ_0. The upper row corresponds to the values $\alpha = -26^\circ$, $\theta_0 = 1/3$ and the lower row to the values $\alpha \approx -15.5^\circ$, $\theta_0 = 1/5$.

the prism by an angle α rotates the beam by 2α). It is pertinent to note that the prism P rotates the complex amplitude of the beam but has a relatively weak effect on the state of beam polarization. The effect of the prism amounts to introducing a slight elliptical polarization into the beam. The intensity of the field component perpendicular to the resonator plane depends on the rotation angle of the prism P and amounts to 0–4% of the intensity of the component lying in the resonator plane. The beam polarization ellipticity takes place only in the portion of the resonator given by $P-M_1-M_2-$active element. In the remaining part of the resonator, the polarization direction is determined by the orientation of the Brewster windows of the active element and lies in the resonator plane. The beam generated by the laser was observed and recorded behind the partially transmitting mirror M_3 with the aid of an objective lens O and a microscope M in the plane of a screen S. The matrix of resonator round trip, beginning with M_1, is given by

$$\begin{pmatrix} A & B \\ C & D \end{pmatrix} = \begin{pmatrix} 1-\dfrac{4l}{R}-\dfrac{2l_0}{R}+\dfrac{4ll_0}{R^2} & 2l+l_0-\dfrac{4l^2}{R}-\dfrac{4ll_0}{R}+\dfrac{4l^2l_0}{R^2} \\ -\dfrac{4}{R}+\dfrac{4l_0}{R^2} & 1-\dfrac{4l}{R}-\dfrac{2l_0}{R}+\dfrac{4ll_0}{R^2} \end{pmatrix} = \begin{pmatrix} -0.939 & 0.446 \\ -0.267 & -0.939 \end{pmatrix}. \quad (31)$$

The beam waist is close to mirror M_1, and the Rayleigh length for this beam is

$$l_R = \frac{B}{\left[1-(A+D)^2/4\right]^{1/2}} \approx 1300 \text{ mm},$$

which corresponds to the Gaussian parameter $w_0 = 0.45$ mm. The phase incursion for the fundamental mode in the empty resonator is $\phi_0 = \arccos(-0.94) \approx 160^\circ$. Therefore, the oscillation frequencies of two neighboring transverse modes differ by 27 MHz for zero angle of prism rotation, and accordingly the frequency separation for two neighboring longitudinal modes is equal to 60 MHz. The transverse mode composition is varied by introducing a thin wire ($W \sim 15$ μm in diameter) into the beam.

The angle of prism rotation P for the self-reproduction of a spiral beam with a rotation parameter θ_0 is

$$\alpha = -\frac{\theta_0}{2}\arccos\frac{A+D}{2} = -\frac{\theta_0}{2}\,2\arccos\sqrt{\left(1-\frac{2l}{R}\right)\left(1-\frac{l_0}{R}\right)} = -\theta_0 \times 79.9^\circ.$$

In the pursuance of experiments, it was discovered that spiral beams for different rotation parameters were realized for a somewhat different value of prism rotation, in particular, for $\alpha = -\theta_0 \times 78^\circ$. This deviation turned out to be similar in all experiments and is supposedly due to the presence of an active medium.

Figure 8 shows the theoretical and experimental results for two spiral beams. Presented in the upper row are the results of experiments in the formation of a spiral beam with the rotation parameter $\theta_0 = 1/3$, $\alpha = -26^\circ$ and the results of numerical calculations for the field $F(r,\phi) = \mathscr{L}_{0,-2}(r,\phi) + 2\mathscr{L}_{0,1}(r,\phi)$. The beam phase has four singularities, or wavefront dislocations, the singularity at the center and those at the periphery being opposite in sign. Given in the lower row are the results of similar experiments for a spiral beam with the rotation parameter $\theta_0 = 1/5$, $\alpha \approx -15.5^\circ$ and numerical calculations for the field $F(r,\phi) = \mathscr{L}_{0,-3}(r,\phi) + 2\mathscr{L}_{0,2}(r,\phi)$. In this case, the beam phase has seven singular points: a z-type singularity of the second order at the center (in the experiment, this singularity is slightly broken) and five $\bar{z}$-type singularities at the periphery.

The possibilities for the realization of different spiral beams in this experiment were limited by reflection and diffraction losses. On the one hand, for large angles of prism rotation (for instance, for beams with $\theta_0 = 1$, $\alpha = -78^\circ$), the angle of beam incidence on the Dove prism is significantly different from the Brewster angle and the losses in the resonator become too big. On the other hand, realization of beams, for instance, with $\theta_0 = 1/4$, requires the presence of Laguerre–Gauss modes $\mathscr{L}_{n_1,m_1}(r,\phi)$ and $\mathscr{L}_{n_2,m_2}(r,\phi)$ with the difference of indices $|m_1 - m_2|$ equal to eight at least, such that diffraction losses in the resonator become significant. Changing the $A+D$ resonator parameter in our experiment was hindered for constructive reasons.

Therefore, spiral beams are the modes of a ring laser with field rotation, which was experimentally confirmed by the intracavity generation of spiral beams with different rotation parameters and a good accord with the results of numerical experiments [58]. The results obtained are demonstration that it is basically possible to produce spiral beams with vastly different spatial characteristics and rotation parameters in a laser with the appropriate resonator and gain of the active medium.

3. Spiral beams with a prescribed intensity distribution

3.1 Beams in the form of plane curves

As noted in the Introduction, the interrelation between the intensity and phase in the one- and two-dimensional cases is radically different. The nonzero curl of the light energy flux vector significantly complicates the relation between the intensity and the phase in this case. At the same time, this complexity generates new possibilities as well.

In particular, it was shown in Section 2.4 that in the two-dimensional case, there exists a class of coherent light fields, referred to as spiral beams, of the form

$$F(x,y,l)=\frac{1}{\sigma}\exp\left(-\frac{x^2+y^2}{\rho^2\sigma}\right)f\left(\frac{x\pm \mathrm{i}y}{\rho\sigma}\right), \tag{32}$$

which retain their structure up to scale and rotation. Here, $f(z)$ is an arbitrary entire analytic function, $\sigma=1+2\mathrm{i}l/k\rho^2$, l is the distance along the beam propagation direction, k is the wavenumber, $\rho=\text{const}$, and the sign in the argument of $f(z)$ determines the direction of beam rotation during propagation.

From this representation, it is clear that the class of fields is rather broad. But to prove the existence of such beams with a predetermined intensity and to define a constructive method for producting them are nontrivial tasks. This section is dedicated to a feasibility study of the purposeful synthesis of beams (32) (see also Ref. [59]).

The structural intensity stability of spiral beams (32) for all l allows us to restrict ourselves, without loss of generality, to the consideration of the beam in the waist plane $l=0$ (which corresponds to $\sigma=1$) and the '+' sign in the argument of f. We introduce the notation

$$\mathscr{S}(z,\bar{z})=\exp\left(-\frac{z\bar{z}}{\rho^2}\right)f\left(\frac{z}{\rho}\right), \tag{33}$$

where $z=x+\mathrm{i}y$ and $\bar{z}=x-\mathrm{i}y$ are complex variables. Then, $\mathscr{S}(z,\bar{z})$ defines the spiral beam $F(x,y,l)$ in the $l=0$ plane and its evolution during propagation. In the subsequent discussion, we therefore refer to $\mathscr{S}(z,\bar{z})$ as the spiral beam (32).

We consider several properties of this class of spiral beams, which follow from representation (33) and are used in what follows.

Property A. If $\mathscr{S}_n(z,\bar{z})=\exp(-z\bar{z}/\rho^2)\,f_n(z/\rho)$ is a collection of spiral beams, their linear combination $\mathscr{S}(z,\bar{z})=\sum_n c_n\mathscr{S}_n(z,\bar{z})$ is also a spiral beam. Moreover, if

$$\mathscr{S}(z,\bar{z},a)=\exp\left(-\frac{z\bar{z}}{\rho^2}\right)f\left(\frac{z}{\rho}\,,\,a\right)$$

is a parametric family of spiral beams, $\mathscr{S}(z,\bar{z})=\int\mathscr{S}(z,\bar{z},a)\,\mathrm{d}a$ is also a spiral beam.

Property B. If $\mathscr{S}_0(z,\bar{z})=\exp(-z\bar{z}/\rho^2)\,f(z/\rho)$ is a spiral beam, then

$$\mathscr{S}(z,\bar{z})=\exp\left(-\frac{z\bar{z}}{\rho^2}\right)f\left(\frac{z\exp(-\mathrm{i}\alpha)}{\rho}\right)$$

is a spiral beam with the same intensity distribution as $\mathscr{S}_0(z,\bar{z})$ but rotated by the angle α.

Property C. If $\mathscr{S}_0(z,\bar{z})=\exp(-z\bar{z}/\rho^2)\,f(z/\rho)$ is a spiral beam, then

$$\mathscr{S}(z,\bar{z})=\exp\left(-\frac{z\bar{z}-2z\bar{z}_0+z_0\bar{z}_0}{\rho^2}\right)f\left(\frac{z-z_0}{\rho}\right) \tag{34}$$

is a spiral beam that has the same intensity distribution as $\mathscr{S}_0(z,\bar{z})$ but is shifted to the point z_0. In this case, in contrast to property B, the change of variable $z\to z-z_0$ does not lead immediately to the desired result. It is easy to see that

$$\exp\left[-\frac{(z-z_0)(\bar{z}-\bar{z}_0)}{\rho^2}\right]f\left(\frac{z-z_0}{\rho}\right)$$
$$=\exp\left(-\frac{z\bar{z}-\bar{z}z_0-z\bar{z}_0+z_0\bar{z}_0}{\rho^2}\right)f\left(\frac{z-z_0}{\rho}\right)$$

is not a spiral beam, because it contains the factor $\exp(\bar{z}z_0/\rho^2)$. Multiplication with the linear phase function $\exp\left[-(\bar{z}z_0-z\bar{z}_0)/\rho^2\right]$ has no effect on the intensity distribution and leads to spiral beam (34).

For $f(z)\equiv 1$, spiral beam (34) becomes an 'elementary spiral beam'

$$\mathscr{S}_{z_0}(z,\bar{z})=\exp\left(-\frac{z\bar{z}-2z\bar{z}_0+z_0\bar{z}_0}{\rho^2}\right), \tag{35}$$

which has a Gaussian intensity distribution shifted to the point z_0. The beam phase is a linear function of coordinates and the beam, of course, travels along a straight line. In this connection, it is instructive to consider how its 'rotation' is realized during propagation. Using representation (32), it is easily found that the trajectory of the intensity peak of beam (35) in the (x,y,l) space is expressed as

$$x+\mathrm{i}y=z_0|\sigma|\exp(\mathrm{i}\arg\sigma)=(x_0+\mathrm{i}y_0)\left(1+\frac{2\mathrm{i}l}{k\rho^2}\right), \tag{36}$$

where x_0 and y_0 are the coordinates of the intensity peak z_0 for $l=0$.

We consider several 'elementary spiral beams' for $|z_0|=\text{const}$. It follows from (35) that in the (x,y,l) space, the trajectories of the peaks of the beams — straight lines — form the surface of a one-sheet hyperboloid of revolution

$$x^2+y^2-\frac{4|z_0|^2}{k^2\rho^4}\,l^2=|z_0|^2\,.$$

The trajectories of the peaks of individual beams and their location on the hyperboloid surface are shown in Fig. 9. For the spiral beams of the general form considered in Section 2.4, the motion trajectories of the points emanating for $l=0$ from the z_0 point also lie in this hyperboloid surface during beam propagation and are helices in the general case.

It is of interest to compare spiral beams with coherent states $|\alpha\rangle$ in quantum mechanics and optics [60]. For instance, in the space $L_2(\mathbf{R}^2)$, the scalar product of 'elementary' spiral

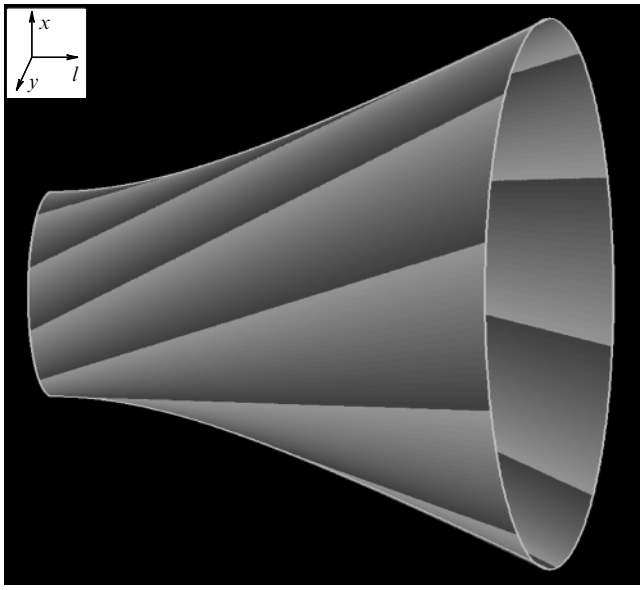

Figure 9. Paths of the peak points of Gaussian beams (35) — straight lines — for $|z_0| = \text{const}$ and their position on the surface of a single-sheet hyperboloid.

beams

$$(\mathscr{S}_{z_0}, \mathscr{S}_{z_1}) = \frac{1}{2}\,\pi\rho^2 \exp\left(-\frac{|z_0|^2 - 2\bar{z}_0 z_1 + |z_1|^2}{\rho^2}\right)$$

is similar to the scalar product of coherent states

$$\langle\alpha|\,\beta\rangle = \exp\left[-\frac{1}{2}\left(|\alpha|^2 - 2\bar{\alpha}\beta + |\beta|^2\right)\right].$$

In a more general case, where

$$\mathscr{S}(z,\bar{z}) = \exp\left(-\frac{z\bar{z}}{\rho^2}\right) f\left(\frac{z}{\rho}\right)$$

is some spiral beam, we have

$$(\mathscr{S}, \mathscr{S}_{z_0}) = \frac{1}{2}\,\pi\rho^2 \mathscr{S}(z_0)\,.$$

For coherent states, this is analogous to the equality $\langle\alpha|\psi\rangle = \exp\left(-|\alpha|^2/2\right)\psi(\bar{\alpha})$, where $|\psi\rangle = \sum_{n=0}^{\infty} c_n|n\rangle$. There also exists a relation between the astigmatic spiral-beam transformation and the coherent states in the coordinate representation and the Fock – Bargman representation, which are considered below.

Using property A for the summation of the Gaussian beam of form (35) shifted to different points, it is now possible to form structurally stable light fields with new properties. The simplest example of this kind is provided by the beam

$$\mathscr{S}\left(z,\bar{z}|[-T,T]\right) = \int_{-T}^{T} \mathscr{S}_t(z,\bar{z})\,\mathrm{d}t = \\ = \exp\left(-\frac{z\bar{z}}{\rho^2}\right)\int_{-T}^{T} \exp\left(-\frac{t^2}{\rho^2} + \frac{2zt}{\rho^2}\right)\mathrm{d}t\,, \qquad (37)$$

which corresponds to an everywhere dense filling of real line segment $[-T, T]$ on complex plane with beams of form (35) (Fig. 10). The beam exhibits a Gaussian decrease in any direction outside the line segment $[-T, T]$, and almost all of the beam energy for $\rho \ll T$ is concentrated in a small neighborhood of this line segment.

From expression (37), in view of properties B and C, it is easy to obtain a spiral beam with the intensity distribution in the form of an arbitrary segment $[z_1, z_2]$ on a complex plane. Let

$$z_0 = \frac{1}{2}(z_1 + z_2)\,, \qquad T = \frac{1}{2}|z_2 - z_1|\,, \qquad \alpha = \arg(z_2 - z_1)\,.$$

Then, the mapping $z \to z_0 + z\exp(\mathrm{i}\alpha)$ transfers the segment $[-T, T]$ to the segment $[z_1, z_2]$. The beam corresponding to the $[z_1, z_2]$ segment is therefore of the form

$$\mathscr{S}\left(z,\bar{z}|[z_1,z_2]\right) = \exp\left(-\frac{z\bar{z} - 2z\bar{z}_0 + z_0\bar{z}_0}{\rho^2}\right) \\ \times \int_{-T}^{T} \exp\left[-\frac{t^2}{\rho^2} + \frac{2t(z - z_0)\exp(-\mathrm{i}\alpha)}{\rho^2}\right]\mathrm{d}t\,. \qquad (38)$$

The $[z_1, z_2]$ segment is referred to as the generating segment for spiral beam (38). On the straight line containing the $[z_1, z_2]$ segment, the complex amplitude of the beam at a point $z_c = cz_1 + (1 - c)z_2$ is

$$\mathscr{S}\left(z_c,\bar{z}_c|[z_1,z_2]\right) = \exp\left[\mathrm{i}\,\frac{(2c-1)\,\mathrm{Im}\,z_1\bar{z}_2}{\rho^2}\right] \\ \times \int_{-c|z_2-z_1|}^{(1-c)|z_2-z_1|} \exp\left(-\frac{t^2}{\rho^2}\right)\mathrm{d}t\,.$$

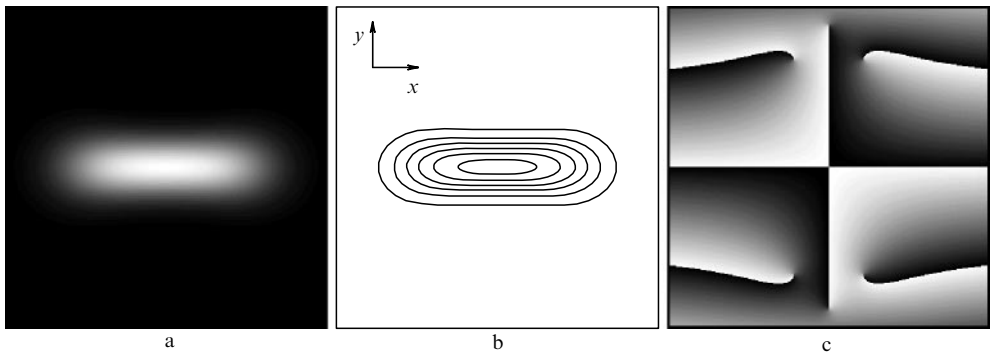

Figure 10. Intensity (a), intensity level lines (b), and phase (c) of a spiral beam in the form of a segment $[-T, T]$. The phase distribution exhibits the presence of six singularities; the central point is not a zero: the presence of only black and white colors in its neighborhood indicates that splicing of the $\varphi = 0$ and $\varphi = 2\pi$ phases occurs.

Therefore, at points of the straight line $z_c = cz_1 + (1-c)z_2$ that are symmetric about the point $(z_1+z_2)/2$, the spiral beam $\mathscr{S}(z,\bar{z}|[z_1,z_2])$ assumes complex conjugate values. In particular, at the ends of the $[z_1,z_2]$ segment,

$$\mathscr{S}(z_1,\bar{z}_1|[z_1,z_2]) = \overline{\mathscr{S}}(z_2,\bar{z}_2|[z_1,z_2]) = \exp\left(\mathrm{i}\,\frac{\operatorname{Im} z_1\bar{z}_2}{\rho^2}\right)\int_0^{|z_2-z_1|}\exp\left(-\frac{t^2}{\rho^2}\right)\mathrm{d}t\,. \tag{39}$$

Owing to a strong localization of beams (38) for $\rho \ll T$ in the vicinity of the segments realized, the interference of such beams manifests in summation only slightly if the segments are sufficiently widely separated. Therefore, the intensity distribution of the field, which is an assembly of such beams, is close to the sum of their intensity distributions.

We now consider contiguous segments $[a,b]$ and $[b,c]$ located on the real axis. Here, the corresponding spiral beams 'seamlessly' merge into one:

$$\mathscr{S}(z,\bar{z}|[a,c]) = \mathscr{S}(z,\bar{z}|[a,b]) + \mathscr{S}(z,\bar{z}|[b,c])\,.$$

Generally, when two segments $[z_1,z_2]$ and $[z_2,z_3]$ lie along a common straight line, it follows from representation (38) that the similar merging of the beams $\mathscr{S}(z,\bar{z}|[z_1,z_2])$ and $\mathscr{S}(z,\bar{z}|[z_2,z_3])$ is given by

$$\mathscr{S}(z,\bar{z}|[z_1,z_3]) = \exp\left(-\mathrm{i}\,\frac{\operatorname{Im}\bar{z}_2z_3}{\rho^2}\right)\mathscr{S}(z,\bar{z}|[z_1,z_2]) + \exp\left(-\mathrm{i}\,\frac{\operatorname{Im}\bar{z}_2z_1}{\rho^2}\right)\mathscr{S}(z,\bar{z}|[z_2,z_3])\,, \tag{40}$$

i.e., phase matching of the constituent beams is required for a smooth beam merging. From expressions (39) and (40), it follows that the phases of the components at the merging point z_2 are

$$\arg\left[\exp\left(-\mathrm{i}\,\frac{\operatorname{Im}\bar{z}_2z_3}{\rho^2}\right)\mathscr{S}(z_2,\bar{z}_2|[z_1,z_2])\right] = \arg\left[\exp\left(-\mathrm{i}\,\frac{\operatorname{Im}\bar{z}_2z_1}{\rho^2}\right)\mathscr{S}(z_2,\bar{z}_2|[z_2,z_3])\right].$$

Therefore, considering the beam $\mathscr{S}(z,\bar{z}|[z_1,z_2]) + \exp(\mathrm{i}\phi)\mathscr{S}(z,\bar{z}|[z_2,z_3])$ for $\phi \in [0,2\pi)$, the uniformity of the total intensity along the segment $[z_1,z_3]$ is highest when

$$\phi = \arg\mathscr{S}(z_2,\bar{z}_2|[z_1,z_2]) - \arg\mathscr{S}(z_2,\bar{z}_2|[z_2,z_3]) = \frac{\operatorname{Im}\bar{z}_2(z_3-z_1)}{\rho^2}\,. \tag{41}$$

Equality (41) may be accepted as the condition of merging two 'segment' beams optimized from the intensity uniformity standpoint, when the points z_1, z_2, and z_3 lie along a straight line. It is noteworthy that equality (41) may be satisfied up to $2\pi N$ (N is an integer), because it expresses the relation between the arguments of complex exponentials.

We now assume that the points z_1, z_2, and z_3 do not lie along a straight line. We apply the phase-matching considerations to the construction of a spiral beam that has the form of a broken line $[z_1,z_2]\cup[z_2,z_3]$. Numerical experiments showed

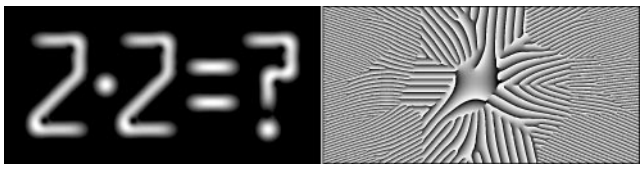

a b

Figure 11. Intensity (a) and phase (b) of a beam constructed of basis spiral beams.

that the intensity distribution of the beam

$$\mathscr{S}(z,\bar{z}|[z_1,z_2]\cup[z_2,z_3]) = \mathscr{S}(z,\bar{z}|[z_1,z_2]) + \exp\left(\mathrm{i}\,\frac{\operatorname{Im}\bar{z}_2(z_3-z_1)}{\rho^2}\right)\mathscr{S}(z,\bar{z}|[z_2,z_3]) \tag{42}$$

along the broken line being formed is rather uniform for different angles between the links $[z_1,z_2]$ and $[z_2,z_3]$. Therefore, phase matching is a useful approach to constructing spiral beams that realize different broken lines. Formula (42) is easily generalized to multilink broken lines.

Using the beams described above as the basis ones, it is possible to construct a wide variety of fields structurally stable against focusing and propagation. An example of a field involving all kinds of such basis beams is given in Fig. 11. According to property B, a spiral beam acquires an additional linear phase under displacement, and therefore the basis beams in this figure, which have equal intensities, have different phase distributions.

The above results bring up the following natural question. Let there be some flat curve defined in the complex-parametric form $\zeta = \zeta(t)$, where the parameter t runs over some interval $[0,T]$. Does there exist a spiral beam $\mathscr{S}(z,\bar{z}|\zeta(t), t\in[0,T])$ that is in the form of this curve? Naturally, the expression 'a beam in the form of the curve $\zeta(t)$' implies the existence of some selection criterion. But for the time being, we do not enlarge on the rigorous mathematical formulation, assuming that a purely visual resemblance would be the desired result. Namely, the intensity of the desired beam should be as high as possible at points z lying in the curve $\zeta(t)$ and as low as possible at the remaining points of the plane.

We construct the spiral beam $\mathscr{S}(z,\bar{z}|\zeta(t), t\in[0,T])$ as the limiting case of the beams that realize the broken lines approximating the curve $\zeta(t)$. Let the parameter t of the $\zeta(t)$ curve vary from 0 to T, $\{kT/n, k=0,1,\ldots,n\}$ be the partition of the segment $[0,T]$, and $\{\zeta_k=\zeta(kT/n), k=0,1,\ldots,n\}$ be its corresponding partition of the curve $\zeta(t)$ (Fig. 12). We consider the approximation of the curve $\zeta(t)$ by the broken line

$$\bigcup_{k=0}^{n-1}[\zeta_k,\zeta_{k+1}] = [\zeta_0,\zeta_1]\cup[\zeta_1,\zeta_2]\cup\ldots\cup[\zeta_{n-1},\zeta_n]$$

and the collection of 'segment' beams $\mathscr{S}(z,\bar{z}|[\zeta_k,\zeta_{k+1}])$ realizing the individual links of this broken line.

Using representation (42) for a two-link broken line, we write the spiral beam for a multilink approximating broken line:

$$\mathscr{S}\left(z,\bar{z}\,\middle|\,\bigcup_{k=0}^{n-1}[\zeta_k,\zeta_{k+1}]\right) = \sum_{k=0}^{n-1}\exp(\mathrm{i}\phi_k)\mathscr{S}(z,\bar{z}|[\zeta_k,\zeta_{k+1}])\,. \tag{43}$$

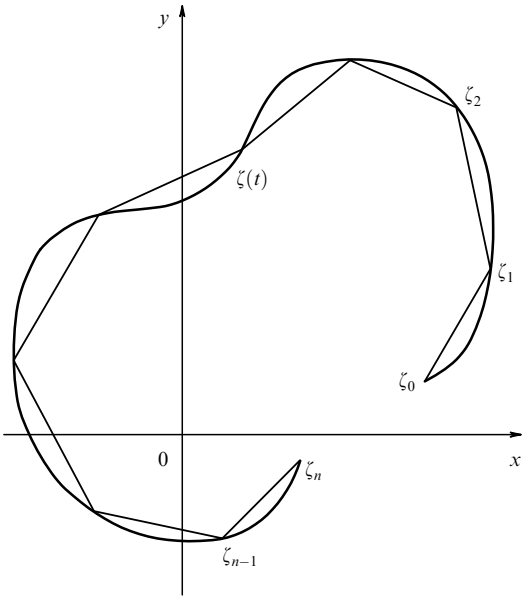

Figure 12. A curve $\zeta(t)$ and its approximating broken line.

Here, $\phi_0 = 0$ and the remaining constants ϕ_k serve to match the phases at the points ζ_k. The phase matching condition for each pair of beams that realize segments having a common point is as follows:

$$\phi_{k-1} + \arg \mathscr{S}\big(\zeta_k, \bar{\zeta}_k | [\zeta_{k-1}, \zeta_k]\big) = \phi_k + \arg \mathscr{S}\big(\zeta_k, \bar{\zeta}_k | [\zeta_k, \zeta_{k+1}]\big)\,, \qquad k = 1, \ldots, n-1\,.$$

We solve this system and use equality (39) to obtain

$$\begin{aligned}\phi_k &= \sum_{j=1}^{k} \left[\arg \mathscr{S}\big(\zeta_j, \bar{\zeta}_j | [\zeta_{j-1}, \zeta_j]\big) - \arg \mathscr{S}\big(\zeta_j, \bar{\zeta}_j | [\zeta_j, \zeta_{j+1}]\big)\right] \\ &= \frac{1}{2\mathrm{i}\rho^2} \sum_{j=1}^{k} \left[\bar{\zeta}_j(\zeta_{j+1} - \zeta_{j-1}) - \zeta_j(\bar{\zeta}_{j+1} - \bar{\zeta}_{j-1})\right], \qquad k = 1, \ldots, n-1\,.\end{aligned}$$

Substituting these expressions in expression (43) and letting the length of each link of the broken line tend to zero yields

$$\begin{aligned}\mathscr{S}\big(z, \bar{z} | \zeta(t), t \in [0, T]\big) &= \lim_{n\to\infty} \mathscr{S}\left(z, \bar{z} \middle| \bigcup_{k=0}^{n-1} [\zeta_k, \zeta_{k+1}]\right) \\ &= \lim_{n\to\infty} \sum_{k=0}^{n-1} \exp\left[\frac{T}{\rho^2 n} \sum_{j=1}^{k} \left(\bar{\zeta}_j \frac{\zeta_{j+1} - \zeta_{j-1}}{2T/n} - \zeta_j \frac{\bar{\zeta}_{j+1} - \bar{\zeta}_{j-1}}{2T/n}\right)\right] \\ &\times \exp\left[-\frac{z\bar{z}}{\rho^2} + \frac{z(\bar{\zeta}_k + \bar{\zeta}_{k+1})}{\rho^2} - \frac{|\zeta_k + \zeta_{k+1}|^2}{4\rho^2}\right] \\ &\times \int_{-|\zeta_{k+1} - \zeta_k|/2}^{|\zeta_{k+1} - \zeta_k|/2} \exp\left\{-\frac{t^2}{\rho^2} + \frac{t(2z - \zeta_k - \zeta_{k+1})}{\rho^2}\right. \\ &\left.\times \exp\left[-\mathrm{i} \arg(\zeta_{k+1} - \zeta_k)\right]\right\} \mathrm{d}t \\ &= \exp\left(-\frac{z\bar{z}}{\rho^2}\right) \lim_{n\to\infty} \frac{T}{n} \sum_{k=0}^{n-1} \exp\left(-\frac{\zeta_k \bar{\zeta}_k}{\rho^2} + \frac{2z\bar{\zeta}_k}{\rho^2}\right) \\ &\times \exp\left[\frac{T}{\rho^2 n} \sum_{j=1}^{k} \left(\bar{\zeta}_j \frac{\zeta_{j+1} - \zeta_{j-1}}{2T/n} - \zeta_j \frac{\bar{\zeta}_{j+1} - \bar{\zeta}_{j-1}}{2T/n}\right)\right] \frac{|\zeta_{k+1} - \zeta_k|}{T/n}\,.\end{aligned}$$

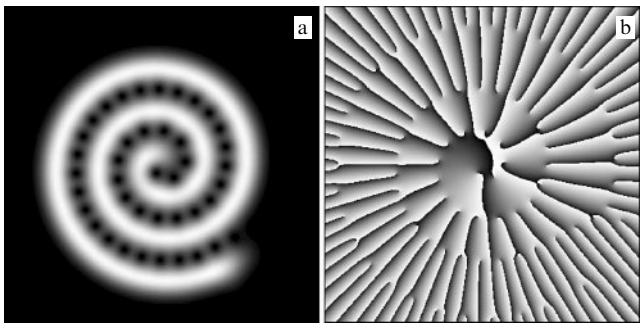

Figure 13. Intensity (a) and phase (b) of a spiral beam in the form of a spiral of Archimedes. Isolated intensity zeroes are seen between the turns.

We consider this expression as the limit of an integral sum. As a result, we arrive at the final formula

$$\begin{aligned}&\mathscr{S}\big(z, \bar{z} | \zeta(t), t \in [0, T]\big) \\ &\quad = \exp\left(-\frac{z\bar{z}}{\rho^2}\right) \int_0^T \exp\left\{-\frac{\zeta(t)\bar{\zeta}(t)}{\rho^2} + \frac{2z\bar{\zeta}(t)}{\rho^2}\right. \\ &\quad \left. + \frac{1}{\rho^2} \int_0^t \left[\bar{\zeta}(\tau)\zeta'(\tau) - \zeta(\tau)\bar{\zeta}'(\tau)\right] \mathrm{d}\tau\right\} \left|\zeta'(t)\right| \mathrm{d}t\,. \qquad (44)\end{aligned}$$

Thus, we have constructed the spiral beam for the curve $\zeta(t)$. How close is its intensity distribution form to the curve $\zeta(t)$?

As is evident from expression (44), the beam is represented in terms of the curve invariants: the differential of arc length $\left|\zeta'(t)\right| \mathrm{d}t$ and the oriented area of the sector swept in tracing the curve

$$\frac{1}{4\mathrm{i}} \int_0^t (\bar{\zeta}\zeta' - \zeta\bar{\zeta}')\, \mathrm{d}\tau\,.$$

That is why the beam is defined by the curve as a geometric object on the plane and, in particular, is independent of its parameterization.

However, in the construction of beam (44), the phase-matching approach was employed for two and only two contiguous links of the broken line and the effect of the remaining ones was neglected. As the length of the links of the broken line is shortened, it is evident that the lengths of the corresponding spiral beams do not tend to zero and their interference becomes stronger. Furthermore, of considerable importance is the curve shape. To exemplify, Fig. 13 shows the beam intensity and phase for the spiral of Archimedes $\zeta(t) = t \exp(\mathrm{i}ct)$. The pitch of the spiral was selected so as to show the interference between its coils. The interference of coils becomes stronger with decreasing the pitch because it becomes comparable to the Gaussian beam parameter ρ.

For closed curves $\zeta(t)$, $t \in [0, T]$, the interference manifests itself in that the construction of spiral beams corresponding to closed broken lines requires matching the phases of the first and last links at the point $\zeta_0 = \zeta_n$.

Therefore, the relation between the curve $\zeta(t)$ and spiral beam (44) is not evident in general. Some aspects of this issue are considered in the next section.

3.2 Properties of beams in the form of closed curves

3.2.1 Quantization condition. Beams for closed curves occupy a separate place and deserve special consideration. Let a function $\zeta(t)$, $t \in [0, T]$ describe a closed curve without self-

intersections. Without loss of generality it may be assumed that the curve is traced in the counterclockwise direction with increasing t. We define $\zeta(t)$ for all real t and continue it periodically outside the segment $[0, T]$. Then, the functions $\zeta(t+a)$, $t \in [0, T]$ describe the same curve for different a. Do the spiral beams for $\zeta(t+a)$ coincide for different a? We show that the beams constructed for closed curves manifest typical quantization properties. First, the intensity distribution of such beams undergoes radical changes under the similarity transformation $\zeta(t) \to v\zeta(t)$ and bears visual resemblance to the curve $v\zeta(t)$ only for specific discrete values of v. Second, only for these v values are the intensities of beams constructed for the curves $v\zeta(t+a)$ the same for different a.

We now find the condition under which the intensities of spiral beams constructed for the curves $\zeta(t)$ and $\zeta(t+a)$ coincide:

$$\left|\mathscr{S}\left(z, \bar{z}|\zeta(t), t \in [a, a+T]\right)\right|^2 \equiv \left|\mathscr{S}\left(z, \bar{z}|\zeta(t), t \in [0, T]\right)\right|^2 .$$

We rewrite this identity as

$$\exp\left[\mathrm{i}\Psi(a)\right]\mathscr{S}\left(z, \bar{z}|\zeta(t), t \in [a, a+T]\right) \equiv \mathscr{S}\left(z, \bar{z}|\zeta(t), t \in [0, T]\right), \tag{45}$$

where $\Psi(a)$ is some real function independent of z [otherwise, canceling the Gaussian function in both sides of identity (45), we obtain Ψ as an analytic function of z, and therefore it cannot be a real function for all z]. We differentiate identity (45) with respect to a and use the periodicity of $\zeta(t)$ to obtain

$$\begin{aligned}
&\exp\left[\mathrm{i}\Psi(a)\right]\mathscr{S}\left(z, \bar{z}|\zeta(t), t \in [a, a+T]\right) \\
&\times \left[\mathrm{i}\Psi'(a) - \frac{\bar{\zeta}(a)\zeta'(a) - \zeta(a)\bar{\zeta}'(a)}{\rho^2}\right] \\
&+ \exp\left[\mathrm{i}\Psi(a) - \frac{z\bar{z} - 2z\bar{\zeta}(a) + \zeta(a)\bar{\zeta}(a)}{\rho^2}\right] \\
&\times \left\{\exp\left[\frac{1}{\rho^2}\int_0^T (\bar{\zeta}\zeta' - \zeta\bar{\zeta}')\,\mathrm{d}\tau\right] - 1\right\}\left|\zeta'(a)\right| = 0 .
\end{aligned}$$

Replacing the spiral beam in the first term in accordance with identity (45) and canceling the Gaussian function, we rewrite this equation in the symbolic form

$$f(z)F_1(a) + \exp\left[\frac{2z\bar{\zeta}(a)}{\rho^2}\right]F_2(a) = 0 ,$$

where $f(z)$ is an entire analytic function and $F_1(a)$ and $F_2(a)$ are some functions of a. This equality is valid for all complex z and real a only if $F_1(a) = F_2(a) \equiv 0$ [if $f(z)$ has a zero, this follows immediately. The case where $f(z)$ has no zeroes is also simple]. Therefore,

$$\Psi(a) = \frac{1}{\mathrm{i}\rho^2}\int_0^a (\bar{\zeta}\zeta' - \zeta\bar{\zeta}')\,\mathrm{d}\tau , \quad \exp\left[\frac{1}{\rho^2}\int_0^T (\bar{\zeta}\zeta' - \zeta\bar{\zeta}')\,\mathrm{d}\tau\right] = 1$$

and consequently [59],

$$\frac{1}{\rho^2}\int_0^T \left[\bar{\zeta}(\tau)\zeta'(\tau) - \zeta(\tau)\bar{\zeta}'(\tau)\right]\mathrm{d}\tau = \frac{4\mathrm{i}S}{\rho^2} = 2\pi\mathrm{i}N ,$$

where S is the area enclosed by the closed contour $\zeta(t)$.

Therefore, the beam intensity is independent of the initial point of integration a only for curves whose surface satisfies the quantization condition

$$S = \frac{1}{2}\,\pi\rho^2 N \qquad (N = 1, 2, \ldots) . \tag{46}$$

The closed curves that satisfy equality (46) are referred to as N-quantized curves and the spiral beams for such curves as N-quantized beams. If we invoke the quantum-mechanical analogy noted in the previous section, the wave functions of a particle in a constant magnetic field in the ground state correspond to spiral beams with $\theta_0 = \pm 1$, $\gamma_0 = 1$. Condition (46) then corresponds to the quantized magnetic flux through the $\zeta(t)$ contour: $\Phi = \left(2\pi\hbar c/|e|\right)N$ (see also Ref. [54]).

Quantization condition (46) is obtained in a natural way as the limiting case of the additional condition for the matching of phases of the first and last links $\phi_{n-1} = \phi_0 + 2\pi N$ in the consideration of closed approximating broken lines [see the note after formula (41)].

Figure 14 shows the intensities and phases of spiral beams in the form of the boundaries of a regular triangle and a square. In calculating the field (44) for the triangle, the hypocycloid

$$\zeta(t) = \mathrm{i}v\rho\left[2\exp(\mathrm{i}t) + \frac{1}{2}\exp(-2\mathrm{i}t)\right], \qquad t \in [0, 2\pi]$$

was taken as the generating curve $\zeta(t)$. The value $v = \sqrt{N/7}$ corresponds to the N-quantized curve. The generating curve for the square is the epicycloid

$$\zeta(t) = \mathrm{i}v\rho\left[3\exp(\mathrm{i}t) - \frac{7}{20}\exp(-3\mathrm{i}t)\right], \qquad t \in [0, 2\pi] ,$$

and the N-quantized curve is obtained for $v = \sqrt{200N/3453}$. The spiral beams shown in Fig. 14 were constructed for the 7-quantized hypocycloid and the 8-quantized epicycloid. The respective areas of the regions enclosed by these curves are $(7/2)\pi\rho^2$ and $4\pi\rho^2$. The phase distributions exhibit the presence of singularities (isolated intensity zeroes), which number 7 and 8 inside the corresponding regions.

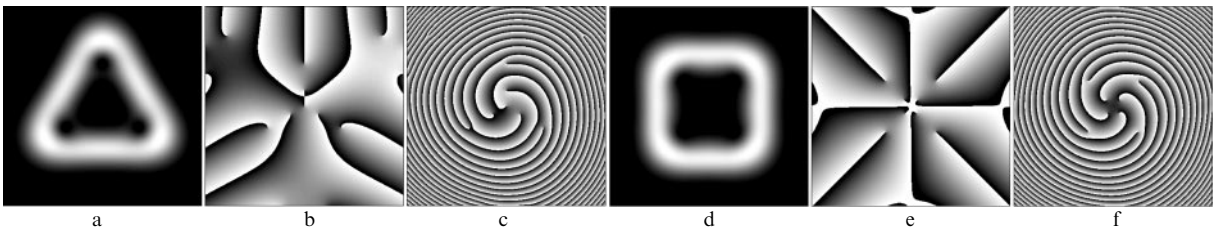

Figure 14. Distribution of the intensity (a, d) and phase (b, e), as well as the phase outside the beam waist (c, f), for spiral beams in the form of boundaries of a regular triangle and a square.

3.2.2 Spiral beam intensity and phase on the generating curve. The beams constructed for quantized curves have a characteristic property. Let $\zeta(t)$, $t \in [0, T]$, be a closed curve satisfying condition (46). Then,

$$\mathscr{S}\big(\zeta(t_0), \bar{\zeta}(t_0)|\zeta(t), t \in [0, T]\big) \neq 0$$

for all $t_0 \in [0, T]$. In other words, the entire function

$$f(z) = \int_0^T \exp\left[-\frac{\zeta(t)\bar{\zeta}(t)}{\rho^2} + \frac{2z\bar{\zeta}(t)}{\rho^2} + \frac{1}{\rho^2}\int_0^t (\bar{\zeta}\zeta' - \zeta\bar{\zeta}')\,\mathrm{d}\tau\right]|\zeta'(t)|\,\mathrm{d}t$$

has no zeroes on the quantized curve $z \in \zeta(t)$, $t \in [0, T]$.

To analyze this statement, we use the saddle-point technique [43] to consider the asymptotic behavior of the beams $\mathscr{S}(z, \bar{z}|v\zeta_1)$ for large values of the parameter v, where ζ_1 is an arbitrary 1-quantized curve without self-intersections. Hereinafter, we use a simplified notation $\mathscr{S}(z, \bar{z}|\zeta)$ for the spiral beam whenever the curve ζ requires no detailing.

We make the change $z \to vz$. Then,

$$\mathscr{S}(vz, v\bar{z}|v\zeta_1) = v\int_0^T \exp\left[-\frac{v^2}{\rho^2}\,P(t)\right]|\zeta_1'(t)|\,\mathrm{d}t\,, \qquad (47)$$

where the complex function $P(t)$ is

$$P(t) = z\bar{z} - 2z\bar{\zeta}_1(t) + \zeta_1(t)\bar{\zeta}_1(t) - \int_0^t \left[\bar{\zeta}_1(\tau)\zeta_1'(\tau) - \zeta_1(\tau)\bar{\zeta}_1'(\tau)\right]\mathrm{d}\tau\,.$$

The saddle-point equation

$$P'(t) = 2\bar{\zeta}_1'(t)\big[\zeta_1(t) - z\big] = 0\,,$$

owing to the absence of singular points [$\bar{\zeta}_1'(t) \neq 0$ for all t] and self-intersections [$\zeta_1(t_1) \neq \zeta_1(t_2)$ for $t_1 \neq t_2$ and $t_1, t_2 \in [0, T)$], has solutions only for $z \in \zeta_1(t)$, $t \in [0, T]$. Let $z = \zeta_1(t_0)$ for some $t_0 \in [0, T]$ and let $v = \sqrt{n} \gg \rho$. Then, $\sqrt{n}\,\zeta_1(t)$ is an n-quantized curve. Because $t = t_0$ is the only saddle point (and a nondegenerate one),

$$\mathscr{S}\big(\sqrt{n}\,\zeta_1(t_0), \sqrt{n}\,\bar{\zeta}_1(t_0)|\sqrt{n}\,\zeta_1\big) = \sqrt{\pi}\,\rho\exp\left[\frac{n}{\rho^2}\int_0^{t_0}(\bar{\zeta}_1\zeta_1' - \zeta_1\bar{\zeta}_1')\,\mathrm{d}\tau\right] + O\left(\frac{1}{n}\right). \qquad (48)$$

As is seen from expression (48), in the limit $n \to \infty$, the intensity tends to $\pi\rho^2$, and therefore

$$\mathscr{S}\big(\sqrt{n}\,\zeta_1(t_0), \sqrt{n}\,\bar{\zeta}_1(t_0)|\sqrt{n}\,\zeta_1\big) \neq 0$$

beginning with some n (which depends, of course, on the form of the curve ζ_1). We note that the intensity distribution on the curve $\sqrt{n}\,\zeta_1(t)$ becomes progressively more uniform with increasing n, and the absence of saddle points for $z \notin \{\zeta_1(t), t \in [0, T]\}$ is responsible for a drop in the spiral-beam intensity outside the curve $\sqrt{n}\,\zeta_1(t)$. Therefore, the asymptotic behavior of the spiral-beam intensity provides a rigorous physical substantiation for the expression 'a beam in the form of the curve $\zeta(t)$'.

For $v \neq \sqrt{n}$ [i.e., for the nonquantized curve $v\zeta_1(t)$], the asymptotic estimate is similar to formula (48) when the point t_0 is not located in the immediate vicinity of boundary points. However, if $t_0 = T$ (or $t_0 = 0$), the intergrand in (47) is not T-periodic and the integration range $[0, T]$ cannot be replaced with $[t_0 - T/2, t_0 + T/2]$. That is why the points $t = 0$ and $t = T$ should be regarded as two different solutions of the saddle-point equation, and the asymptotic estimate becomes

$$\mathscr{S}\big(v\zeta_1(T), v\bar{\zeta}_1(T)|v\zeta_1\big) = \sqrt{\pi}\,\rho\,\frac{1 + \exp(2\pi\mathrm{i}v^2)}{2} + O\left(\frac{1}{v^2}\right). \qquad (49)$$

This expression implies that for $v \neq \sqrt{n}$, the intensity on the curve $v\zeta_1(t)$ does not tend to the constant $\pi\rho^2$ as $v \to \infty$ and, in addition, the location of intensity nonuniformity on the curve $v\zeta_1(t)$ is determined by the initial point of integration. Figure 15 shows the possibilities for the intensity distribution of a nonquantized triangular-shaped spiral beam in relation to the choice of the initial point of the integration range.

We emphasize once again the asymptotic nature of the resultant expressions. A more detailed analysis of formula (48) allows reinforcing the statement about the order of magnitude of the remainder term. However, the issue of a rigorous proof of the condition

$$\mathscr{S}\big(\sqrt{n}\,\zeta_1(t_0), \sqrt{n}\,\bar{\zeta}_1(t_0)|\sqrt{n}\,\zeta_1\big) \neq 0 \quad \text{for all} \quad n \geqslant 1 \qquad (50)$$

still remains open. Even when the quantization condition is fulfilled, the expression on the left-hand side of the last inequality is inseparable from zero (i.e., the zero constant cannot be replaced with a slightly larger one). The main problem consists in the efficient use of the condition for the absence of self-intersection points on the generating curve.[5]

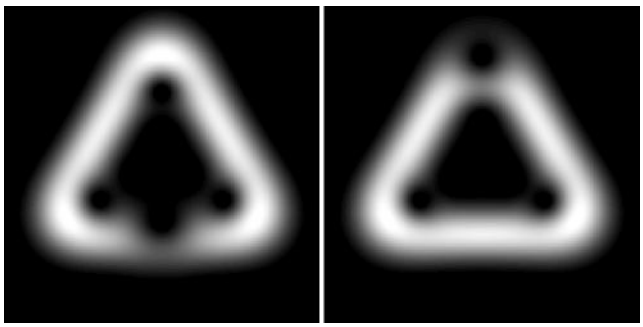

a b

Figure 15. Intensities of spiral beams (44) constructed for the nonquantized triangular-shaped hypocycloid

$$\zeta(t) = 1.0425\mathrm{i}\rho\left[2\exp(\mathrm{i}t) + \frac{1}{2}\exp(-2\mathrm{i}t)\right]$$

and different integration intervals: (a) $t \in [-\pi, \pi]$, (b) $t \in [0, 2\pi]$. The parameter 1.0425 lies between 1 and $\sqrt{8/7}$, which corresponds to the intermediate position between the 7- and 8-quantized curves.

[5] The simplicity of the formulation of this condition cannot be underestimated. Reference [61] was concerned with the following problem: What shape should a rectangular band of paper have to allow making a Moebius strip? It is clear that the band should be narrow and long (there is no way of making a Moebius strip, for instance, out of a square sheet). The search for the minimal possible length-to-width ratio for the band led to the following result:

$$\frac{\pi}{2} \leqslant \inf\frac{\text{length}}{\text{width}} \leqslant \sqrt{3}\,.$$

However, the exact equality was not found, because no answer was provided to the same old question as to how use should be made of the condition for the absence of self-crossings.

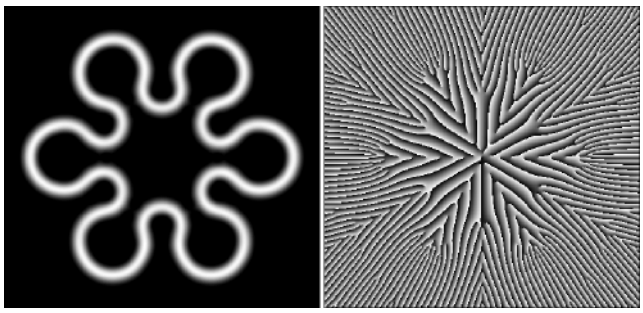

a b

Figure 16. Intensity (a) and phase (b) of a spiral beam constructed for a 97-quantized curve in the form of a snowflake.

To illustrate this difficulty, Fig. 16 gives an example of a spiral beam. Where portions of the curve nearly touch each other, the existing zeroes approach the generating curve quite closely, and it is only the condition for the absence of self-crossings that prevents the zeroes from settling themselves in the curve itself and thereby transforming (50) into an equality.

3.2.3 The number of spiral-beam zeroes inside the domain enclosed by the generating curve. We consider the circulation of the phase gradient of the quantized beam $\mathscr{S}(z,\bar{z}|\sqrt{N}\zeta_1) = \sqrt{I(x,y)}\exp\left[\mathrm{i}\varphi(x,y)\right]$ along its generating contour. As suggested by Refs [4, 46] and noted in the Introduction,

$$\oint_{\sqrt{N}\zeta_1} \nabla\varphi\,\mathrm{d}\mathbf{r} = 2\pi\sum_n \operatorname{sgn}\operatorname{rot}_0\mathbf{j}(z_n)\,, \tag{51}$$

where the scalar function

$$\operatorname{rot}_0\mathbf{j} = \frac{1}{k}\left(\frac{\partial I}{\partial x}\frac{\partial\varphi}{\partial y} - \frac{\partial I}{\partial y}\frac{\partial\varphi}{\partial x}\right)$$

is the longitudinal component of the curl of the light energy flux vector $\mathbf{j}$ and the summation is performed over all zeroes z_n of the spiral beam residing within the contour $\sqrt{N}\zeta_1(t)$, counted with multiplicities. [6]

For spiral beams (44), as for general beams (33), $\operatorname{rot}_0\mathbf{j}(z_n) = -\operatorname{sgn}\theta_0 = 1$, and therefore

$$\oint_{\sqrt{N}\zeta_1} \nabla\varphi\,\mathrm{d}\mathbf{r} = 2\pi N_0\,,$$

where N_0 is the number of zeroes of the beam $\mathscr{S}(z,\bar{z}|\sqrt{N}\zeta_1)$ inside the contour $\sqrt{N}\zeta_1(t)$, counted with multiplicities.

We show that

$$N_0 = N\,. \tag{52}$$

Because $N = 2S/\pi\rho^2$, equality (52) relates the number of quantized-beam zeroes in the domain enclosed by the generating curve to the area of the domain itself.

Forestalling the proof, we consider the construction of spiral beams in the form of a circle. Using representation (44) and neglecting the insignificant constant factor that emerges as a result of integration, we obtain the expression

$$\mathscr{S}\left(z,\bar{z}|R\exp(\mathrm{i}t),\ t\in[0,2\pi]\right) = \exp\left(-\frac{z\bar{z}}{\rho^2}\right)\sum_{n=0}^{\infty}\frac{\sin(2R^2/\rho^2-n)\pi}{2R^2/\rho^2-n}\,\frac{(-2zR/\rho^2)^n}{n!}\,.$$

From the quantization condition for the circle $S = \pi R^2 = \pi\rho^2 N/2$, it follows that $2R^2/\rho^2 = N$, and the series reduces to the single Nth term:

$$\mathscr{S}\left(z,\bar{z}\left|\rho\sqrt{\frac{N}{2}}\exp(\mathrm{i}t),\ t\in[0,2\pi]\right.\right) = \exp\left(-\frac{z\bar{z}}{\rho^2}\right)\left(\frac{z}{\rho}\right)^N. \tag{53}$$

Therefore, quantized spiral beams for a circle are the well-known Laguerre – Gauss beams. The validity of equality (52) is evident in this case.

We now assume that there exists some N-quantized curve $\hat{\zeta}(t)$ for which equality (52) is not fulfilled. Then, we construct a family of closed curves $\zeta(t,c)$ that depends on the parameter $c\in[0,1]$, begins with the N-quantized curve

$$\zeta(t,0) = \rho\sqrt{\frac{N}{2}}\exp(\mathrm{i}t)\,,$$

ends with the curve $\zeta(t,1) = \hat{\zeta}(t)$, and has a fixed area of the enclosed domain $S = \pi\rho^2 N/2$ for every curve $\zeta(t,c)$. This ensures fulfillment of quantization condition (46) for all $c\in[0,1]$ for a continuous deformation of the circle. However, the spiral beam for the circle satisfies condition (52) and the spiral beam for the $\hat{\zeta}(t)$ curve does not. The number of zeroes of the N-quantized spiral beam $\mathscr{S}\left(z,\bar{z}|\zeta(t,c)\right)$ in the domain enclosed by the contour $\zeta(t,c)$ should therefore change for some c. The following reasoning applies for the mechanism of the spiral-beam zero number variation under changes in the generating curve. The zeroes of the spiral beam are zeroes of the corresponding analytic function. From the principle of maximum modulus [40], it follows that the modulus of the analytic function does not have a minimum inside the domain, provided this minimum is not a zero of the function. Consequently, no zero can arise from the minimum of the function modulus or be transformed to a minimum inside the domain under changes in the parameter c, because there exists no such minimum for an analytic function. The variation of the number of zeroes therefore results from the penetration of a zero into the domain enclosed by the contour $\zeta(t,c)$ from outside or vice versa. In this case, however, there exists a parameter value $c = c_0$ such that the spiral beam $\mathscr{S}\left(z,\bar{z}|\zeta(t,c_0)\right)$ has a zero on the contour $\zeta(t,c_0)$, which is impossible, as noted above.

Therefore, to a quantized beam, there corresponds a well-defined number of phase singularities inside the domain enclosed by the generating curve, which depends on the area of the domain and not on its shape [59]. Hence, it follows that changing the domain area, for instance, from $S = \pi\rho^2 N/2$ to $S = \pi\rho^2(N+1)/2$ leads to an increase in the number of zeroes inside the domain via arrival of one zero from outside. Figure 17 shows the evolution of the spiral beam for the circle $\zeta(t) = R\exp(\mathrm{i}t)$, $t\in[0,2\pi]$ for $2R^2/\rho^2\in[4,0;5,0]$ and makes the process of zero penetration inside the contour evident. The limited dimensions of the

[6] If z_n is a degenerate zero, then $\operatorname{rot}_0\mathbf{j}(z_n) = 0$ and formula (51) requires a more precise definition. The function $\operatorname{rot}_0\mathbf{j}(z)$ for spiral beams (32) may be shown to be of constant signs in the small neighborhood of the point z_n. By $\operatorname{sgn}\operatorname{rot}_0\mathbf{j}(z_n)$ in this case, we mean $\lim_{z\to z_n}\operatorname{sgn}\operatorname{rot}_0\mathbf{j}(z)$.

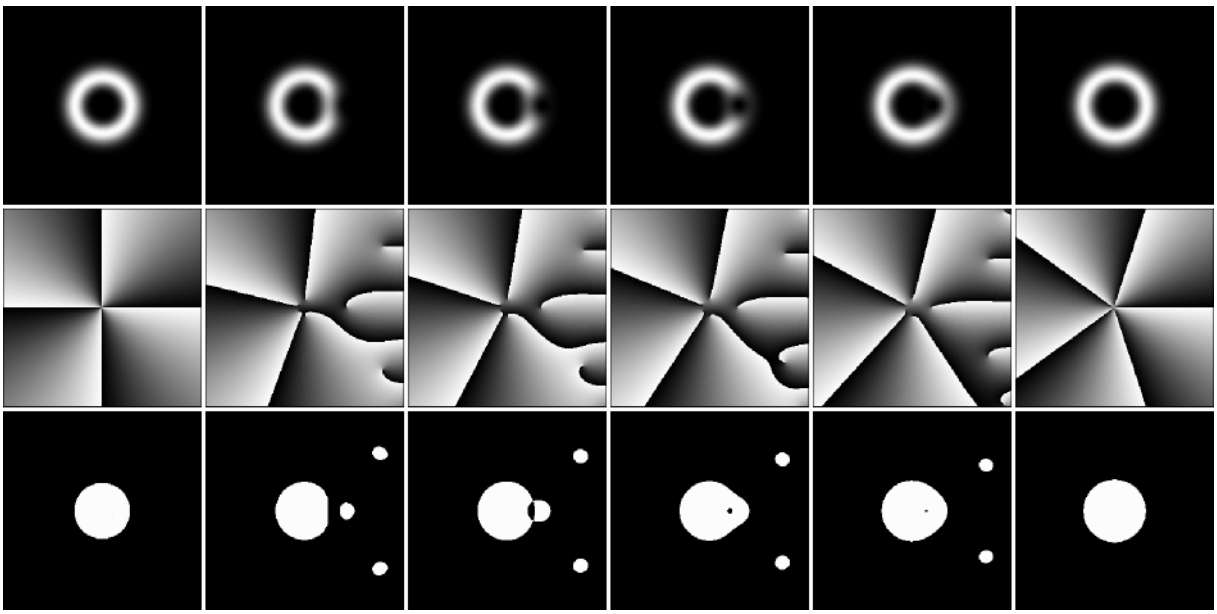

Figure 17. Evolution of the spiral beam under changes in the radius of the generating circle: intensity (upper row), phase (middle row), and sign of the curl $\mathrm{rot}_0\,\mathbf{j}$ of light energy flux vector (lower row). Black color corresponds to negative values of the curl and white color to positive ones.

graphic images give us no way of seeing what occurs at the periphery simultaneously with the changes at the ring center. With an increase in the radius R of the generating circle, when the spiral beam ceases to be quantized and the degenerate zero at the center breaks up into four simple ones, a wedge of zeroes forms at infinity, which approach these four progressively closer as R increases. The zero located at the wedge end penetrates the interior of the circle enclosed by the generating circle, while the rest of the zeroes remain outside. After that, the internal quintuple of zeroes begins to draw together and, simultaneously, the wedge of zeroes, which has lost one of its representatives, begins to recede from them. When the spiral beam becomes quantized again, the zeroes at the center merge into a fifth-order zero and the wedge at infinity disappears. The region of zero penetration, as mentioned above, is determined by the initial point of integration.

3.2.4 Spiral beams for symmetric curves. The symmetry of closed curves shows up in the properties of the corresponding spiral beams. Let a curve $\zeta(t)$, $t\in[0,2\pi]$ be mapped into itself under rotation by the angle $2\pi/M$, i.e., $\zeta(t+2\pi/M)=\zeta(t)\exp(2\pi\mathrm{i}/M)$. Then, the quantized spiral beams $\mathscr{S}(z,\bar z|\zeta_n)$ constructed for the corresponding quantized curves $\zeta_n(t)$ have the following properties:

(a) $\mathscr{S}\bigl(z\exp(2\pi\mathrm{i}/M),\bar z\exp(-2\pi\mathrm{i}/M)|\zeta_n\bigr)=\mathscr{S}(z,\bar z|\zeta_n)\times\exp(2\pi\mathrm{i}n/M)$;

(b) $\mathscr{S}(z,\bar z|\zeta_n)$ has a zero of multiplicity $n-[n/M]M$ at $z=0$. If $n\geqslant M$, the remaining zeroes located inside the contour $\zeta_n(t)$ are situated at the vertices of regular M-gons (one or several). For instance, $M=3$ for the hypocycloid $\triangle_7$:

$$\zeta(t)=\mathrm{i}\rho\left[2\exp(\mathrm{i}t)+\frac{1}{2}\exp(-2\mathrm{i}t)\right],\qquad t\in[0,2\pi]\,.$$

The beam $\mathscr{S}(z,\bar z|\triangle_7)$ therefore contains a simple zero at $z=0$ and six other zeroes at the vertices of two regular triangles (see Figs 14a–c);

(c) if $n-m$ is not divisible by M, the beams $\mathscr{S}(z,\bar z|\zeta_n)$ and $\mathscr{S}(z,\bar z|\zeta_m)$ are orthogonal in the space $L_2(\mathbf{R}^2)$. In the case of a circle, for instance, for M, one can take an arbitrarily large natural number. Therefore, $\mathscr{S}(z,\bar z|\bigcirc_n)$ and $\mathscr{S}(z,\bar z|\bigcirc_m)$ are orthogonal for all $n\neq m$. This result is well known, because it is a special case of the orthogonality of Laguerre–Gauss modes.

3.2.5 Spiral beams as generalizations of Laguerre–Gauss modes. According to expression (53), the Laguerre–Gauss modes $\mathscr{L}_{0,n}(x,y)=\exp(-x^2-y^2)(x+\mathrm{i}y)^n$ are a special case of quantized spiral beams when a circle is selected as the generating curve. The entire family of Laguerre–Gauss modes can be obtained in terms of generating curves. For this, we rewrite expression (20) for $l=0$ as

$$\begin{aligned}\mathscr{S}_m(z,\bar z)&=\exp(Z\bar Z)\,\frac{\partial^m}{\partial Z^m}\bigl(\exp(-2Z\bar Z)\,f(Z)\bigr)\\&=\left(\rho\,\frac{\partial}{\partial z}-\frac{\bar z}{\rho}\right)^m\mathscr{S}(z,\bar z)\,,\end{aligned}\tag{54}$$

where $z=x+\mathrm{i}y$, $Z=z/\rho$, $\mathscr{S}(z,\bar z)=\exp(-z\bar z/\rho^2)f(z/\rho)$, and in lieu of N use is made of the symbol m. We note that the operator acting on $\mathscr{S}(z,\bar z)$ is the creation operator for the Hamiltonian that describes particle motion in a uniform magnetic field [62].

Substitution of the spiral beam corresponding to the n-quantized circle

$$\mathscr{S}\bigl(z,\bar z|\bigcirc_n\bigr)=\exp\left(-\frac{z\bar z}{\rho^2}\right)\left(\frac{z}{\rho}\right)^n,$$

for $\mathscr{S}(z,\bar z)$ gives, up to a constant factor, the Laguerre–Gauss modes of the general form

$$\mathscr{S}_m\bigl(z,\bar z|\bigcirc_n\bigr)=\mathscr{L}_{\min(m,n),n-m}\left(\frac{x}{\rho},\frac{y}{\rho}\right).$$

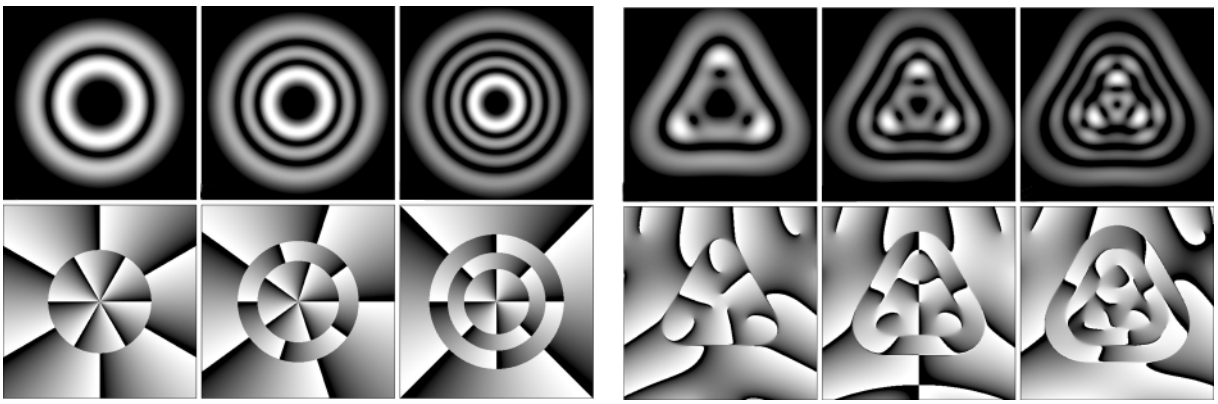

Figure 18. Intensities and phases of the Laguerre – Gauss beams $\mathscr{L}_{m,7-m}(x,y)$ and the spiral beams $\mathscr{S}_m(z,\bar{z}|\triangle_7)$ for $m=1,2,3$.

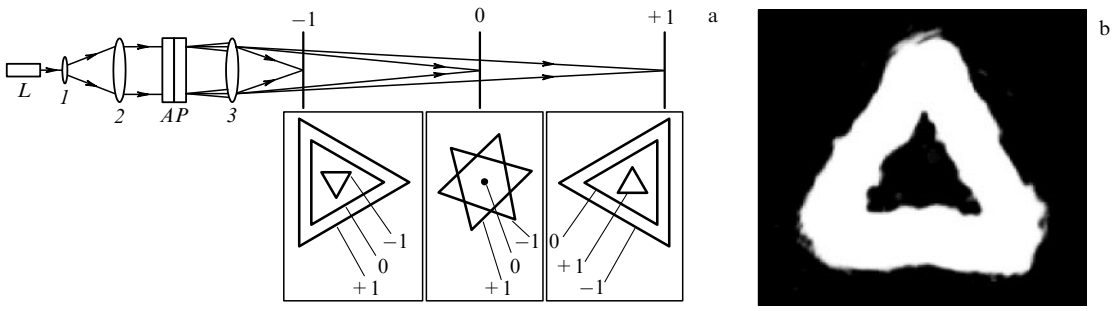

Figure 19. Schematic layout of the experiment for synthesizing a spiral beam in the form of the boundary of a regular triangle (a) and the recorded intensity distribution in the +1 diffraction order (b).

Therefore, spiral beams in the form of closed curves can be regarded as a generalization of Laguerre – Gauss beams $\mathscr{L}_{0,n}(x,y)$. We can continue this analogy and construct, for every generating curve, a family of spiral beams corresponding to the complete family of Laguerre – Gauss beams. To do this, we choose the field $\mathscr{S}(z,\bar{z})$ in representation (54) to be an n-quantized spiral beam in the form of an arbitrary generating curve $\zeta(t)$. Then, the resultant field assumes the form

$$\mathscr{S}_m(z,\bar{z}|\sqrt{n}\,\zeta_1)=\left(\rho\,\frac{\partial}{\partial z}-\frac{\bar{z}}{\rho}\right)^m\mathscr{S}(z,\bar{z}|\sqrt{n}\,\zeta_1)\,. \tag{55}$$

Here, as before, $\zeta_1(t)$ is a 1-quantized curve. As the initial beam $\mathscr{S}(z,\bar{z}|\sqrt{n}\,\zeta_1)$, the beams (55) rotate during propagation, because they have the same rotation parameter $\theta_0=-1$. Furthermore, they inherit the features of the generating curve. Laguerre – Gauss beams and the corresponding spiral beams for a 7-quantized hypocycloid of triangular form are exemplified in Fig. 18. Interestingly, in contrast to Laguerre – Gauss beams, low-intensity lines are no longer zero lines and this intensity structure is ensured only by isolated zeroes, which are rather complicated in form and which imitate zero-intensity lines.

3.3 Methods of synthesis of structurally stable beams with a predetermined intensity distribution

3.3.1 Amplitude – phase mask technique. Spiral beams (44) were experimentally realized in the following way [59]. Computer-calculated amplitude half-tone masks for the amplitude and phase were made with a photoplotter (a resolution of 1024×1024 elements, dimensions of 10×10 mm). The amplitude mask for the phase was employed to fabricate a phase element on dichromated gelatin. The combination of the amplitude A and phase P masks yield the requisite amplitude – phase distribution. To realize a triangle-shaped spiral beam (Figs 14a, c), use was made of the phase distribution plotted in Fig. 14c, because its spatial frequency is higher than that of the distribution shown in Fig. 14b. Furthermore, a quadratic phase addition with the wavefront curvature 0.002 mm^{-1} was superimposed on the phase distribution at the beam waist to increase the diffraction efficiency of the phase element.

The experiment is schematized in Fig. 19a. The beam of a laser L is expanded and illuminates an amplitude – phase element AP (the element was rotated by 90° in comparison to the distribution plotted in Fig. 14). A lens *3* ($f=250$ mm) focuses the +1st, 0th, and −1st diffraction orders onto the +1st, 0th, and −1st planes, respectively. The diffraction efficiency in these orders was as follows: $\eta_1:\eta_2:\eta_3\approx10:7:3$, $\eta_1\approx40\%$. The intensity distribution patterns in the planes 0 and ±1 is schematically shown in the lower part of the figure. The spiral beams rotating in the opposite directions, $\mathscr{S}_{+1}=\exp(-z\bar{z})f(z)$, $\mathscr{S}_{-1}=\exp(-z\bar{z})\overline{f(z)}$, are realized in the orders +1 and −1. Observed in the zero order is the ordinary pattern of diffraction from the amplitude transparency A. This field is not a spiral beam and does not retain its structure under focusing on the plane 0. Figure 19b shows the experimental intensity distribution in the diffraction order +1 in the plane +1.

3.3.2 Astigmatic transformation technique. We now consider another way of realizing spiral beams in the form of curves, which involves astigmatic transformation (26) of Hermite –

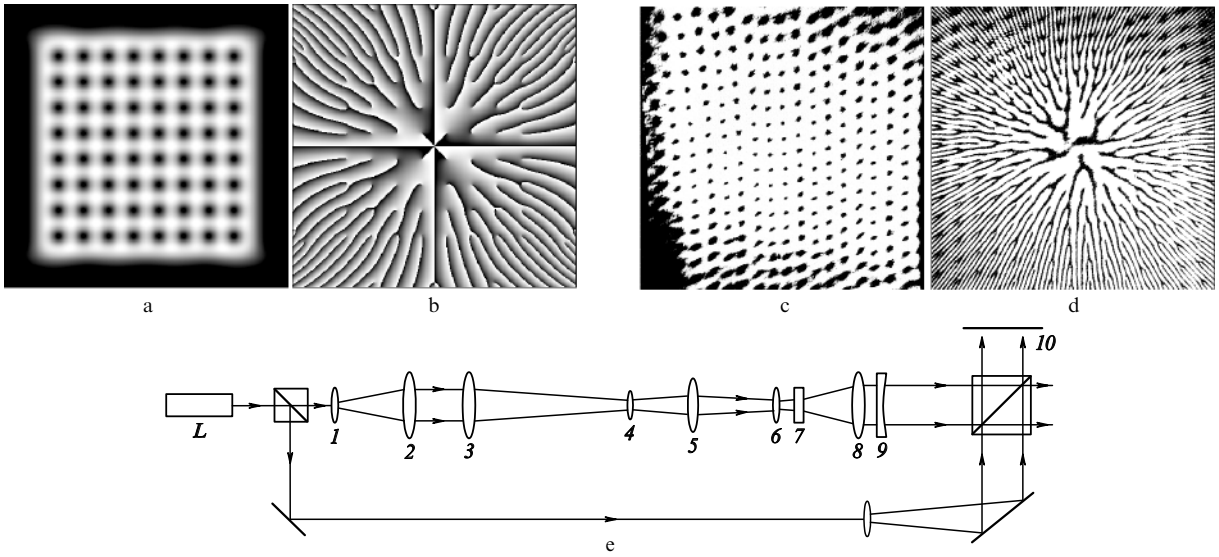

Figure 20. Theoretical calculations and experimental realization of spiral beams in the form of an array of zeroes and the as optical scheme (e) for the synthesis of such beams. Intensity (a) and phase (b) of the spiral beam $\mathscr{S}(z,\bar{z}|\boxplus_{8\times 8})$ (theory); intensity (c) and the result of interference between the spiral and reference beams (d) (experiment).

Gauss beams to Laguerre–Gauss beams. Its special case

$$\iint_{\mathbf{R}^2} \exp\left[-\mathrm{i}(x\xi+y\eta)+\frac{2\mathrm{i}\xi\eta}{\rho^2}\right]\mathscr{H}_{n,0}\left(\frac{\xi}{\rho},\frac{\eta}{\rho}\right)\mathrm{d}\xi\,\mathrm{d}\eta = \frac{\pi\rho^2}{\sqrt{2}}(-2\mathrm{i})^n\exp\left(-\frac{\mathrm{i}\rho^2xy}{4}\right)\mathscr{L}_{0,n}\left(\frac{\rho x}{2\sqrt{2}},\frac{\rho y}{2\sqrt{2}}\right)$$

allows synthesizing the spiral beams $\exp(-z\bar{z})z^n$ and can be generalized as follows:

$$\iint_{\mathbf{R}^2} \exp\left[-\mathrm{i}(x\xi+y\eta)+\frac{2\mathrm{i}\xi\eta}{\rho^2}-\frac{\eta^2}{\rho^2}\right]g\left(\frac{\xi}{\rho}\right)\mathrm{d}\xi\,\mathrm{d}\eta = \sqrt{\pi}\,\rho^2\exp\left(-\frac{\mathrm{i}\rho^2xy}{4}\right)\mathscr{S}\big(\rho(x+\mathrm{i}y),\rho(x-\mathrm{i}y)\big)\,. \quad (56)$$

Here, $g(\xi)\in L_2(\mathbf{R})$ and the spiral beam $\mathscr{S}(z,\bar{z})$ is given by

$$\mathscr{S}(z,\bar{z}) = \exp\left(-\frac{1}{8}\,z\bar{z}+\frac{1}{8}\,z^2\right)\int_{\mathbf{R}}\exp(-\xi^2-\mathrm{i}z\xi)\,g(\xi)\,\mathrm{d}\xi\,.$$

The following sequence of operations may be suggested for the experimental synthesis of spiral beams with the use of transformation (56):

(a) to form the light field $\exp(-\eta^2/\rho^2)g(\xi/\rho)$ for some function $g(\xi)$;

(b) to perform the astigmatic transformation of this field;

(c) to compensate for the astigmatism after the transformation.

For instance, for $g(\xi)=\mathrm{rect}\,(\xi/a)$, a spiral beam 'line segment' similar to that depicted in Fig. 10 is realized. Then, the resultant spiral beam for

$$g(\xi)=\mathrm{rect}\left(\frac{\xi}{a}\right)\sum_{n=-N}^{N}\exp(\mathrm{i}n\omega\xi)$$

has the shape of $2N+1$ parallel vertical-beam 'line segments':

$$\mathscr{S}_N(z,\bar{z}) = \sum_{n=-N}^{N}\exp\left(-\frac{1}{8}\,z\bar{z}+\frac{1}{8}\,z^2\right)\times\int_{-a}^{a}\exp\big[-\xi^2-\mathrm{i}\xi(z-n\omega)\big]\,\mathrm{d}\xi\,. \quad (57)$$

For $\omega\sim\omega_0=2\sqrt{\pi}$, separate beams 'stick together' and beam (57) takes the form of an array of zeroes that are symmetric with respect to x, y (Figs 20a, b). The frequency ω_0 is obtained from the following considerations. For $a\gg 1$ and $N\to\infty$, beam (57) can be represented as

$$\mathscr{S}_\infty(z,\bar{z}) = \sqrt{\pi}\exp\left(-\frac{1}{8}\,z\bar{z}-\frac{1}{8}\,z^2\right)\times\sum_{n=-\infty}^{\infty}\exp\left(-\frac{1}{4}\,\omega^2n^2+\frac{1}{2}\,\omega zn\right).$$

Here, the series is the theta function ϑ_3. Setting $\omega=\omega_0$ and using the Poisson resummation formula for this theta function [63],

$$\sum_{n=-\infty}^{\infty}\exp(-\pi n^2+2\mathrm{i}nz) = \exp\left(-\frac{z^2}{\pi}\right)\sum_{n=-\infty}^{\infty}\exp(-\pi n^2+2nz)\,,$$

we obtain the symmetric property and periodicity of the intensity:

$$\big|\mathscr{S}_\infty(z,\bar{z})\big|^2=\big|\mathscr{S}_\infty(\mathrm{i}z,-\mathrm{i}\bar{z})\big|^2=\big|\mathscr{S}_\infty(z+\omega_0,\bar{z}+\omega_0)\big|^2 = \big|\mathscr{S}_\infty(z+\mathrm{i}\omega_0,\bar{z}-\mathrm{i}\omega_0)\big|^2\,.$$

The beam described by (57) was realized with the aid of a Damman array with a spatial frequency ω_0 as a multiplication element. The experiment is schematically represented in Fig. 20e. The beam emanating from a laser L is expanded and collimated by spherical lenses *1*, *2*. Cylindrical lenses *3*, *4* compress the beam in one direction and, in combination with an astigmatic transformer comprising spherical *5* and cylindrical *6* lenses, produce the field $\exp(-\eta^2/\rho^2)\,\mathrm{rect}\,(\xi/a)\exp(2\mathrm{i}\xi\eta/\rho^2)$. Placed immediately behind cylindrical lens 6 was diffraction lattice *7*, which produced 17 orders of equal intensity. Astigmatic transformation (56) was realized in the Fraunhofer zone behind the lattice and the intensity distribution of the output beam looked like an array of zeroes. A combination of long-focus

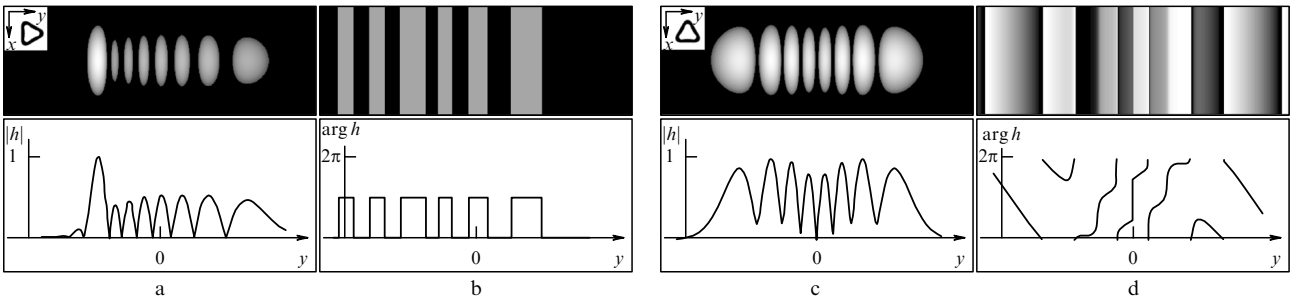

Figure 21. Amplitude–phase elements for a spiral beam of triangular shape vs. the rotation angle of the generating curve.

collecting *8* and diverging *9* lenses compensated for the astigmatism at the transformer output. The second arm of the scheme was used for the interferometric visualization of the phase of the spiral beam on screen *10*. The reference front curvature selected was then equal to the curvature of the beam at the transformer output. The experimental results are given in Figs 20c, d. As can be seen from Fig. 20d, at every isolated zero, there occurs interference fringe branching, which corresponds to a phase singularity at this point. At all intensity zeroes, the values of the curl of the light energy flux vector are of the same sign (have the same topological charge). The structural distortion of the vortex array in the experiment in comparison with the theoretical distribution arises from some residual aberrations.

Astigmatic transformation can underlie yet another method, kindred to the previous one, of spiral beam formation. Let $\mathscr{S}_m(z,\bar{z})$ be a beam of form (54). Then, the equality

$$\iint_{\mathbf{R}^2} \exp\left[-\mathrm{i}(x\xi+y\eta)+\frac{2\mathrm{i}\xi\eta}{\rho^2}\right]\mathscr{S}_m(\xi+\mathrm{i}\eta,\xi-\mathrm{i}\eta)\,\mathrm{d}\xi\,\mathrm{d}\eta = \frac{\pi\rho^2}{\sqrt{2}}\left(\frac{\mathrm{i}}{\rho}\right)^m \exp\left(-\frac{\mathrm{i}\rho^2xy}{4}-\frac{\rho^2x^2}{8}\right)H_m\left(\frac{\rho x}{2}\right)h(y) \qquad (58)$$

holds, where $H_m(t)$ is the Hermite polynomial and

$$h(y)=\frac{1}{\sqrt{\pi}}\exp\left(-\frac{\rho^2y^2}{8}\right)\int_{\mathbf{R}}\exp(-t^2)\,f\left(\frac{\rho y}{2}+\mathrm{i}t\right)\mathrm{d}t\,. \qquad (59)$$

It is easily seen that all information on the spiral beam structure is contained in $h(y)$, which is a function of one variable. Therefore, this function effects a peculiar one-dimensional coding of the two-dimensional spiral beam.

We set $m=0$ in formula (58) and take the spiral beam $\mathscr{S}(z,\bar{z}|\zeta)$ in the form of the curve $\zeta(t)$, with the result that the function h assumes the form

$$h(y|\zeta)=\exp\left(-\frac{\rho^2y^2}{8}\right)\int_0^T\exp\left[-\frac{\bar{\zeta}^2(t)}{\rho^2}-\frac{\zeta(t)\bar{\zeta}(t)}{\rho^2}+y\bar{\zeta}(t)+\frac{1}{\rho^2}\int_0^t(\bar{\zeta}\zeta'-\zeta\bar{\zeta}')\,\mathrm{d}\tau\right]\left|\zeta'(t)\right|\mathrm{d}t\,.$$

In particular, for a quantized circle, we obtain the one-dimensional Hermite–Gauss mode[7]

$$h(y|\bigcirc_n)=\exp\left(-\frac{\rho^2y^2}{8}\right)H_n\left(\frac{\rho y}{2}\right).$$

[7] It is interesting to note the occurrence of this function in formula (58).

The following method can be proposed for the synthesis of spiral beams with the use of coder functions:

(a) to synthesize a one-dimensional amplitude–phase element $h(y)$;

(b) to 'reconstruct' the spiral beam intensity with the astigmatic one-dimensional Hermite–Gauss beam

$$\exp\left(-\frac{\mathrm{i}\rho^2xy}{4}-\frac{\rho^2x^2}{8}\right)H_m\left(\frac{\rho x}{2}\right)$$

in the Fraunhofer diffraction zone or in the Fourier plane.

Figure 21 shows the amplitude–phase elements corresponding to spiral beams of triangular shape versus the angle of rotation of the generating curve. The generating curve was chosen as a 7-quantized hypocycloid, for which the spiral beam is shown in Fig. 14. Figures 21a and 21b show the amplitude (a) and phase (b) of the distribution

$$\exp\left(-\frac{\rho^2x^2}{8}\right)h(y|\triangleright_7)\,,$$

as well as the plots of the amplitude and phase of the one-dimensional function $h(y|\triangleright_7)$. Figures 21c and 21d give a similar amplitude–phase element for a 7-quantized hypocycloid rotated by 90°. Unlike the previous distribution, which was purely real, the element $h(y|\triangle_7)$ is complex-valued.

The amplitude–phase element for a spiral beam in the form of an array of zeroes is shown in Fig. 22. We see from Fig. 22 that the coder function for the array of zeroes is real (this can also be proven theoretically). Because the coder function for a quantized circle is also real, any beam in the form of an array of zeroes can be obtained by astigmatic transformation of a product of one-dimensional real functions. The one-dimensional structure of amplitude–phase coder elements enables harnessing the potentialities of microlithography in full measure, and therefore this approach may turn out to be preferable to the amplitude–phase mask method.

To conclude this section, we consider the relation between the resultant beams and several well-known transformations.

1. We turn to astigmatic transformation (56) and rewrite the resultant spiral beam $\mathscr{S}(z,\bar{z})$ as

$$\mathscr{S}(2\mathrm{i}z,-2\mathrm{i}\bar{z})=\exp\left(-\frac{z\bar{z}}{2}\right)\times\int_{\mathbf{R}}\exp\left(-\frac{z^2}{2}+2z\xi-\xi^2\right)g(\xi)\,\mathrm{d}\xi=\exp\left(-\frac{z\bar{z}}{2}\right)f(z)\,.$$

As a result, we have the Gabor transformation [64] of the function $g(\xi)$, where the analytic function $f(z)$ is related to

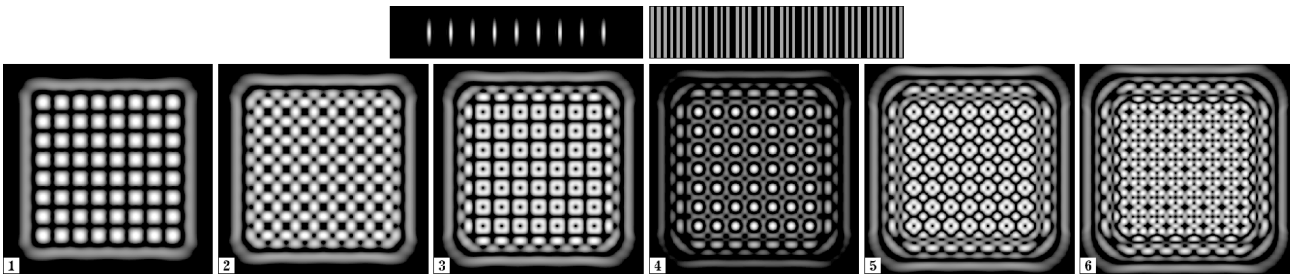

Figure 22. Upper row: amplitude and phase of the coder element for the spiral beam $\mathscr{S}(z,\bar{z}|\boxplus_{8\times8})$ (Figs 20a and 20b). Lower row: intensities of the spiral beams $\mathscr{S}_m(z,\bar{z}|\boxplus_{8\times8})$ constructed by formula (54) for $1 \leqslant m \leqslant 6$.

$g(\xi)$ by the integral transformation with the kernel $\exp(-z^2/2 + 2z\xi - \xi^2)$. Furthermore, in quantum mechanics [60], the relation between the coordinate representation of a state $|q\rangle$ and the Fock–Bargman representation $\langle z|$ is effected by the integral representation with the kernel

$$\langle z|q\rangle = \frac{1}{\sqrt[4]{\pi\hbar}} \exp\left(-\frac{z^2}{2} + \frac{2zq}{\sqrt{2\hbar}} - \frac{q^2}{2\hbar}\right).$$

Therefore, astigmatic transformation (56) realizes the relation between two quantum-mechanical representations by optical means.

2. From transformation (56), there also follows the feasibility of optical realization of the analytic continuation of the Fourier transform of the field $g(\xi)$ through an astigmatic transformation. For instance, for a finite field $g(\xi)$ with the support $[-a, a]$, the sequence of operations is as follows. First, the field $g(\xi)$ is transmitted through the amplitude mask $\exp(-a^2 + \xi^2 - \eta^2)$ and the astigmatic phase element $\exp(2i\xi\eta)$. Effected next is the optical Fourier transform. The zeroes of the output field are the zeroes of the analytic continuation of the Fourier transform of $g(\xi)$. The resultant analytic continuation may be employed as the basis of a new method of phase reconstruction [65].

3. During propagation, the evolution of the field from expression (59),

$$F(x,y,0) = \exp\left(-\frac{\rho^2 y^2}{8}\right) h(\rho x|\zeta),$$

is of the form

$$\begin{aligned} F(x,y,l) &= \frac{k}{2\pi i l}\iint_{\mathbf{R}^2} \exp\left\{\frac{ik}{2l}\left[(x-\xi)^2 + (y-\eta)^2\right]\right\} \\ &\quad \times F(\xi,\eta,0)\,d\xi\,d\eta \\ &= \frac{1}{\sigma}\exp\left[\frac{il\rho^4(x^2+y^2)}{32k|\sigma|^2}\right]\exp\left(-\frac{\rho^2 y^2}{8|\sigma|^2}\right) \\ &\quad \times h\left(\frac{\rho x}{|\sigma|}\middle|\zeta\exp(i\arg\sigma)\right), \end{aligned} \tag{60}$$

where $\sigma = 1 + il\rho^2/4k$. We compare expressions (59) and (60) to find that for every l, the above field $F(x,y,l)$ coincides, up to scale and a phase factor, with the astigmatic transform of the spiral beam $\mathscr{S}(z\exp(-i\arg\sigma), \bar{z}\exp(i\arg\sigma)|\zeta)$, which is obtained from the initial spiral beam by rotation by the angle $\arg\sigma$.

Transformation (60) and the corresponding astigmatic transformation can be given a geometric interpretation. We consider the three-dimensional distribution (see also Refs [56, 59])

$$W(x,u,y) = \exp\left(-\frac{2ixu}{\rho^2} - \frac{2y^2}{\rho^2}\right)\mathscr{S}(x+iu, x-iu|\zeta).$$

The projection of this distribution on the plane $u = 0$ is

$$W_{\mathrm{PR}}(x,y) = \int_{\mathbf{R}} W(x,u,y)\,du = \sqrt{\pi}\exp\left(-\frac{2y^2}{\rho^2}\right) h\left(\frac{4x}{\rho}\middle|\zeta\right).$$

This projection coincides, up to a scale, with $F(x,y,0)$. Accordingly, under rotation of the $W(x,u,y)$ distribution by the angle $\arg\sigma$ about the y axis, its projection on the plane $u = 0$ coincides with $F(x,y,l)$ up to a scale and a phase factor. Therefore, the evolution of the field $F(x,y,l)$ during propagation looks like a change in the projection $W(x,u,y)$ in its rotation about the y axis.

3.4 Synthesis of phase elements for focusing into curves

Owing to their structural stability, spiral beams are always amplitude–phase and not purely phase light fields. Therefore, the methods of light-field synthesis outside a cavity involving a transformation of some initial field by means of amplitude–phase optical elements are inevitably associated with the loss of a significant fraction of the transformed field energy, making these methods nonoptimal for applied problems. At the same time, the structural field stability during propagation and focusing is not always a necessity: it would be quite sufficient to achieve an efficient transformation of the initial light field into the field with a prescribed intensity distribution in some plane. Hence, the problem is naturally formulated in the following way: to 'trade' the structural stability of the spiral beam for the possibility of forming the prescribed intensity distribution in some plane using a purely phase element.

The problem of synthesizing a phase element (the so-called 'focusator') for the formation of light fields with a prescribed intensity distribution is well known and has its own history and bibliography (see, e.g., Ref. [66]). Mathematically, the problem of laser radiation focusing amounts to determination of a piecewise smooth function $\exp[i\varphi(\xi,\eta)]$ such that its Fresnel transform for $l = l_0$ yields the desired intensity distribution $I(x,y)$:

$$\begin{aligned} I(x,y) &= \left|F(x,y)\right|^2 \\ &= \left|\frac{k}{2\pi i l_0}\iint_{\Omega}\exp\left\{\frac{ik}{2l_0}\left[(x-\xi)^2 + (y-\eta)^2\right]\right\}\right. \\ &\quad \left.\times\exp\left[i\varphi(\xi,\eta)\right]d\xi\,d\eta\right|^2. \end{aligned} \tag{61}$$

Here, Ω is the aperture of the optical element.

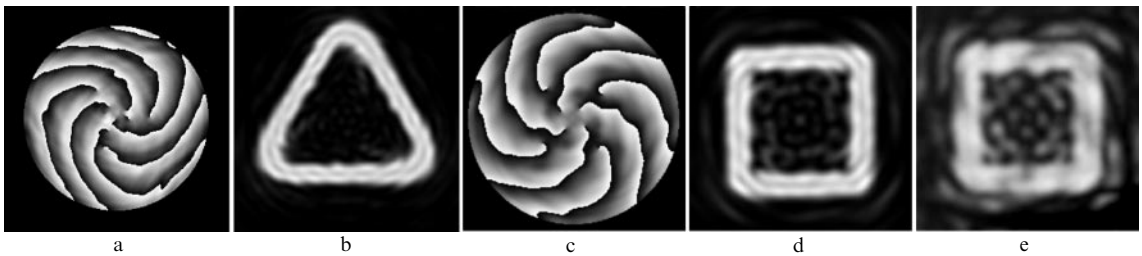

Figure 23. Distribution of the phase of optical elements (a, c) over a circular aperture and distribution of field intensities in the focal region (b, d — theory, e — experiment).

We also emphasize that the expression 'the desired intensity distribution $I(x, y)$' should be interpreted not in the sense of the analytic representation of the function I but somewhat more broadly. For instance, it is evident that the problem of focusing distribution (61) for $I(x, y) = \mathrm{rect}\,(x/a)\,\mathrm{rect}\,(y/b)$ has no solutions for any positive a or b, because the intensity $I(x, y)$ is an entire analytic function in both variables. Nevertheless, the task of focusing into a rectangle with the side ratio a/b is among the most frequently encountered [66, 67].

Therefore, in focusing laser radiation into a curve L (another commonly considered case is a two-dimensional domain), it is assumed that the intensity distribution $I(x, y)$ is maximum at the points of the curve L or size of its ε-neighborhood (the size ε is much shorter than the length of L), while the total fraction of energy within this neighborhood is as close to 100% as possible. Moreover, a more or less uniform intensity distribution over the curve L is yet another significant requirement, which should be taken into account in solving the problem. To summarize the aforesaid, the problem of laser radiation focusing on some curve L may be considered solved when the intensity $I(x, y)$ in the plane $l = l_0$ which results from focusing by an element $\exp\left[\mathrm{i}\varphi(\xi, \eta)\right]$ bears visual resemblance to the curve L itself. Quantitative characteristics — the energy fraction $\iint_{L_\varepsilon} I\,\mathrm{d}x\,\mathrm{d}y / \iint_{\mathbf{R}^2} I\,\mathrm{d}x\,\mathrm{d}y$ (L_ε is the ε-neighborhood of the curve L) and the degree of uniformity $\min_L I / \max_L I$ — characterize the precision of this visual resemblance.

One of the main techniques for the solution of focusing problems for different curves L is the stationary phase approximation [assuming that $k(\mathrm{diam}\,\Omega)^2 \gg 2l_0$]. Its application allows treating the $\varphi(\xi, \eta)$-search problem as the process of mapping the domain Ω in the initial plane onto the curve L in the plane $l = l_0$, with each point $(x, y) \in L$ having an infinite number of preimages in the domain Ω. When such an approximation is employed in optics, the curve L is referred to as a caustic and the investigation itself as the geometric approach to the focusing problem. A rigorous mathematical formulation of the problem of focusing on a curve and its detailed investigation in the framework of geometrical optics were presented in Refs [68, 69]. The approach involving the stationary phase approximation does not yield initial conditions owing to the specific character of the problem, and therefore the solution to the problem is fundamentally ambiguous. The choice of the mapping has a significant effect on the form of the solution $\varphi(\xi, \eta)$ and, as a consequence, on the intensity $I(x, y)$. Within this approximation, the wave properties of the fields being formed escape consideration.

In connection with the aforesaid, the solutions obtained by the stationary phase method are commonly modified to include the wave properties of the light field by one iterative procedure or another, for instance, by the Gerchberg – Saxton technique [70]. It is pertinent to note that the success of this approach depends strongly on the initial approximation obtained, as noted above, by the stationary phase technique. According to Ref. [71], however, the solutions to the focusing problem with phase singularities cannot be derived by the stationary phase technique. In the above-mentioned paper, it was shown by the specific example of the problem of focusing into a ring that there exists an infinite set of solutions that are wave solutions and do not furnish a degenerate mapping of the aperture of an optical element onto a circle. Therefore, they are not 'focusators' from the standpoint of the stationary phase technique. Moreover, the region of wave focusing lies in the geometric shadow domain.

These facts became the starting point for the elaboration of a method of synthesis of phase elements for focusing on curves (which relies on the phase structure of the corresponding spiral beams naturally containing phase singularities) as the initial approximation. Numerical experiments exhibited a very rapid convergence of the method. Figure 23 provides examples of the phase elements found with the use of the corresponding spiral beams and the Gerchberg – Saxton technique and shows the result of their focusing action.

4. Integral characteristics of spiral beams

It is well known [72 – 74] that the energy and angular momentum of any beam remain invariable during propagation in the Fresnel zone, i.e.,

$$E = \iint_{\mathbf{R}^2} \left|F(x, y, l)\right|^2 \mathrm{d}x\,\mathrm{d}y = \mathrm{const}\,,$$

$$L = \frac{1}{E} \iint_{\mathbf{R}^2} M(x, y, l)\,\mathrm{d}x\,\mathrm{d}y = \mathrm{const}$$

are integral invariants. Here,

$$M(x, y, l) = \mathrm{Im}\left[\bar{F}(x, y, l)\left(y\,\frac{\partial F}{\partial x}(x, y, l) - x\,\frac{\partial F}{\partial y}(x, y, l)\right)\right]$$

is the angular momentum density. As noted in the Introduction, investigations of the two-dimensional phase problem revealed that a significant part was played by the vortical component of the light energy flux. Specifically, the complex field amplitude

$$F(x, y, l) = \sqrt{I(x, y, l)}\,\exp\left[\mathrm{i}\varphi(x, y, l)\right]$$

can be reconstructed if the field intensity $I(x, y)$, its directional derivative $\partial I(x, y)/\partial l$, and the projection of the curl of the

light energy flux on the direction of propagation

$$\operatorname{rot}_0 \mathbf{j}(x,y) = \frac{1}{k}\left(\frac{\partial I}{\partial x}\frac{\partial \varphi}{\partial y} - \frac{\partial I}{\partial y}\frac{\partial \varphi}{\partial x}\right)$$

are given in some plane $l = l_0$ in the Fresnel zone.

Generally, attempts to reconstruct the flux curl from intensity measurements do not meet with success. However, some of the properties of the curl are known [4]:

1. If (x_0, y_0) is a point of the intensity extremum and $I(x_0, y_0) \neq 0$, then $\operatorname{rot}_0 \mathbf{j}(x_0, y_0) = 0$. But if $I(x_0, y_0) = 0$, then

$$\left|\operatorname{rot}_0 \mathbf{j}(x_0, y_0)\right| = \frac{1}{k}\sqrt{\frac{\partial^2 I}{\partial x^2}\frac{\partial^2 I}{\partial y^2} - \left(\frac{\partial^2 I}{\partial x\,\partial y}\right)^2}\,.$$

2. If (x_0, y_0) is a simple zero of $F(x, y)$ and C is a contour enclosing only this zero of F, then

$$\oint_C \nabla\varphi \,\mathrm{d}\mathbf{r} = 2\pi \operatorname{sgn} \operatorname{rot}_0 \mathbf{j}(x_0, y_0)\,.$$

3. The principle of vortical component conservation for the field $F(x, y, l)$ holds: the equality

$$\iint_{\mathbf{R}^2} \operatorname{rot}_0 \mathbf{j}(x, y, l)\,\mathrm{d}x\,\mathrm{d}y = 0$$

is valid for any plane in the Fresnel zone. This equality is the special case of a more general property, namely

$$\iint_{\mathbf{R}^2} f(x+\mathrm{i}y)\left(\frac{\partial I}{\partial l}(x,y,l) + \mathrm{i}\operatorname{rot}_0 \mathbf{j}(x,y,l)\right)\mathrm{d}x\,\mathrm{d}y = 0 \quad (62)$$

for any plane in the Fresnel zone and an arbitrary integer analytic function $f(z)$ that does not destroy the convergence of the integral. For beams with a Gaussian decrease at infinity (for instance, for spiral beams), $f(z)$ can be an arbitrary-degree polynomial in z. In particular, the case $f(z) \equiv 1$ gives the already-known conservation laws for the energy and the vortical component of the light energy flux vector.

If $P_n(x, y)$ is a polynomial in the variables x and y of degree $n \geqslant 1$, it can be shown that the integrals

$$\begin{aligned} &\iint_{\mathbf{R}^2} P_n(x,y)\,\frac{\partial I}{\partial l}(x,y,l)\,\mathrm{d}x\,\mathrm{d}y\,,\\ &\iint_{\mathbf{R}^2} P_n(x,y)\operatorname{rot}_0 \mathbf{j}(x,y,l)\,\mathrm{d}x\,\mathrm{d}y \end{aligned} \quad (63)$$

are polynomials in l of the degree $n-1$ or lower. As a consequence, for $n = 1$, both integrals are independent of l and thus are integral invariants for an arbitrary field F. Applying this result to $f(z) = z$ in Eqn (62), it is easy to obtain the invariants

$$\begin{aligned} &\iint_{\mathbf{R}^2} (x+\mathrm{i}y)\operatorname{rot}_0 \mathbf{j}(x,y,l)\,\mathrm{d}x\,\mathrm{d}y = c\,,\\ &\iint_{\mathbf{R}^2} (x+\mathrm{i}y)\,\frac{\partial I}{\partial l}(x,y,l)\,\mathrm{d}x\,\mathrm{d}y = -\mathrm{i}c\,, \end{aligned} \quad (64)$$

which depend on one constant c. The significance of this constant is not evident for an arbitrary field, but it can be elucidated for spiral beams. To do this, we address the properties of displaced spiral beams again and consider how the angular momentum of a spiral beam changes in its displacement. It can be shown that the beams $\mathscr{S}(z, \bar{z})$ obey the optical analog of the Steiner theorem [75]: the angular momentum L_{z_0} of the spiral beam displaced by a value z_0 relative to the initial one satisfies the relation

$$L_{z_0} = L_{z_{\mathrm{init}}} - 2|z_{\mathrm{init}} - z_0|^2\,, \quad (65)$$

where z_{init} are the center-of-gravity coordinates of the initial beam intensity:

$$z_{\mathrm{init}} = -\frac{1}{E}\iint_{\mathbf{R}^2} (x+\mathrm{i}y)\left|\mathscr{S}(z,\bar{z})\right|^2 \mathrm{d}x\,\mathrm{d}y\,.$$

For instance, for an elementary spiral beam whose intensity is in the form of a displaced Gaussian distribution,

$$L\left[\exp\left(-z\bar{z} + 2z\bar{z}_0 - z_0\bar{z}_0\right)\right] = -2|z_0|^2\,.$$

We now return to the constant c in the right-hand sides of equalities (64). By expanding the flux curl in terms of the Hermite – Gauss modes for spiral beams, it can be shown that

$$\iint_{\mathbf{R}^2} (x+\mathrm{i}y)\operatorname{rot}_0 \mathbf{j}(x,y,l)\,\mathrm{d}x\,\mathrm{d}y = \frac{2E}{k}\,z_{\mathrm{init}}\,.$$

Consequently, $c = 2Ez_{\mathrm{init}}/k$ in this case. Because the angular momentum of spiral beams (20) and (21) satisfies the relation $L\left[\mathscr{S}_N(z,\bar{z})\right] = N + L\left[\mathscr{S}(z,\bar{z})\right]$, the Steiner theorem and the last-mentioned relation are also valid for arbitrary beams.

The integrals (63) for $n \geqslant 2$ and the fields of the general form $F(x, y, l)$ were found to be difficult to investigate and the resultant polynomials in l difficult to represent. Nevertheless, the following two results are valid. The first one relates the angular momentum to the curl of the light energy flux:

$$L = \frac{k}{2E}\iint_{\mathbf{R}^2} (x^2+y^2)\operatorname{rot}_0 \mathbf{j}(x,y,l)\,\mathrm{d}x\,\mathrm{d}y\,. \quad (66)$$

To prove this, it suffices to apply the Green formula to the circulation of the vector field $(x^2+y^2)I\nabla\varphi$. The second result consists in the fact that there are no integral invariants for cubic polynomials $P_3(x, y)$.

5. Conclusion

In recent years, the term singular optics has been used in reference to the area of investigation of light fields with wavefront dislocations, or optical vortices. Fields of this kind are produced and observed in both linear and nonlinear optical media and are the subject of rather intensive research, and therefore satisfying the demand for adequate theoretical and experimental approaches to the investigation of fields with optical vortices is a topical problem. Of course, from the formal standpoint, any coherent light field can be represented as a superposition of the well-known Hermite – Gauss and Laguerre – Gauss modes; however, this approach proves to be nonoptimal for the analysis and synthesis of fields with phase singularities.

The vortical fields retaining (up to scale and rotation) their structure during propagation, or the light fields that are the concern of our review, are peculiar 'vortical modes' in the class of fields with phase singularities and merit closer consideration as a subject of coherent optics. In our view,

this is due to the following main reasons. First, being highly diversified in the form of intensity distribution, these beams are nevertheless described by analytic expressions. This makes them an efficient instrument of research of the laws of formation and transformation of light fields with phase singularities of the general form. Second, in quantum mechanics, there is a direct analog for spiral beams – wave functions of a charged particle in a uniform magnetic field and the laws of spiral-beam transformation have a representation in the theory of coherent states. It is not unlikely that these analogies will be mutually beneficial to both quantum mechanics and optics. The third and the last, the possibility of versatile variation of spiral-beam intensity distribution with retention of its structural stability during propagation and focusing is of interest for laser technologies and the development of specific atomic traps, while a nonzero angular momentum of these beams offers fresh opportunities for manipulating microobjects.

Several significant aspects of the optics of spiral beams have not been discussed in our review. In particular, here we considered only beams in the form of curves without self-intersections. The case of curves with self-intersections turned out to be more complicated: for such beams subject to quantization condition (46), for instance, the amplitude zeroes can occur on the generating curve. The beams for curves with self-intersections are the subject of an ongoing study.

It can be shown [76] that the scalar product of the complex amplitudes of spiral beams coincides with the scalar product of the corresponding one-dimensional coder functions. Furthermore, there exist vast classes of mutually orthogonal spiral beams. Hence, it follows that such coder functions may be employed as the kernels of specific wavelet transforms for signal processing [77, 78]. The properties of these wavelet transforms are also currently under investigation.

This work was supported by the Russian Foundation for Basic Research (Grant No. 04-02-96508p-2004), the 'Semiconductor Lasers' Program of the Physical Sciences Division of the Russian Academy of Sciences, the 'Investigations in Priority Areas of Science and Technology' Program of the ministry of Science and Technology, and the 'Basic Research and Higher Education' Russian – American Program (CRDF Grant No. REC-SA-014-02).

References

1. Born M, Wolf E *Principles of Optics* 4th ed. (Oxford: Pergamon Press, 1969) [Translated into Russian (Moscow: Nauka, 1973)]
2. Kogelnik H, Li T *Appl. Opt.* **5** 1550 (1966)
3. Volostnikov V G, Preprint No. 93 (Moscow: Lebedev Physics Institute, 1990); *J. Sov. Laser Res.* **11** 601 (1990)
4. Abramochkin E G, Volostnikov V G *Opt. Commun.* **74** 144 (1989)
5. Korn G A, Korn T M *Mathematical Handbook for Scientists and Engineers* (New York: McGraw-Hill, 1961) [Translated into Russian (Moscow: Nauka, 1968)]
6. Nye J F, Berry M V *Proc. R. Soc. London Ser. A* **336** 165 (1974)
7. Baranova N B, Zel'dovich B Ya *Zh. Eksp. Teor. Fiz.* **80** 1789 (1981) [*Sov. Phys. JETP* **53** 925 (1981)]
8. Baranova N B et al. *Zh. Eksp. Teor. Fiz.* **83** 1702 (1982) [*Sov. Phys. JETP* **56** 983 (1982)]
9. Bazhenov V Yu, Vasnetsov M V, Soskin M S *Pis'ma Zh. Eksp. Teor. Fiz.* **52** 1037 (1990) [*JETP Lett.* **52** 429 (1990)]
10. Bazhenov V Yu, Soskin M S, Vasnetsov M V *J. Mod. Opt.* **39** 985 (1992)
11. Soskin M S et al. *Phys. Rev. A* **56** 4064 (1997)
12. Soskin M S, Vasnetsov M V, in *Progress in Optics* Vol. 42 (Ed. E Wolf) (Amsterdam: Elsevier, 2001) p. 219
13. Ilyenkov A V et al., in *Intern. Conf. on Holography and Correlation Optics, 15–19 May 1995, Chernovtsy, Ukraine* (Proc. SPIE, Vol. 2647, Ed. O V Angelsky) (Bellingham, Wash.: SPIE, 1995) p. 43
14. Bekshaev A Ya et al. *Pis'ma Zh. Eksp. Teor. Fiz.* **75** 155 (2002) [*JETP Lett.* **75** 127 (2002)]
15. Bekshaev A Y, Popov A Y, in *Selected Papers from 5th Inter. Conf. on Correlation Optics, 10–13 May 2001, Chernivtsi, Ukraine* (Proc. SPIE, Vol. 4607, Ed. O V Angelsky) (Bellingham, Wash.: SPIE, 2002) p. 90
16. Alekseev K N, Volyar A V, Fadeeva T A *Opt. Spektrosk.* **93** 639 (2002) [*Opt. Spectrosc.* **93** 588 (2002)]
17. Freund I *Opt. Commun.* **181** 19 (2000)
18. Dana I, Freund I *Opt. Commun.* **136** 93 (1997)
19. Heckenberg N R et al. *Opt. Quantum Electron.* **24** S951 (1992)
20. Schechner Y Y, Piestun R, Shamir J *Phys. Rev. E* **54** R50 (1996)
21. Heckenberg N R et al. *Opt. Lett.* **17** 221 (1992)
22. He H et al. *Phys. Rev. Lett.* **75** 826 (1995)
23. Heckenberg N R et al. *Phys. Rev. A* **54** 2369 (1996)
24. Basistiy I V et al. *Pis'ma Zh. Eksp. Teor. Fiz.* **76** 566 (2002) [*JETP Lett.* **76** 486 (2002)]
25. Basistiy I V et al. *Opt. Lett.* **28** 1185 (2003)
26. Soskin M S (Ed.) *Intern. Conf. on Singular Optics, 5–10 October 1997, Partenit, Ukraine* (Proc. SPIE, Vol. 3487) (Bellingham, Wash.: SPIE, 1998)
27. Soskin M S, Vasnetsov M V (Eds) *2nd Intern. Conf. on Singular Optics, 2–6 October 2000, Crimea, Ukraine* (Proc. SPIE, Vol. 4403) (Bellingham, Wash.: SPIE, 2001)
28. Berry M, Dennis M, Soskin M (Eds) "Special issue on singular optics: Selected papers from the NATO Advanced Research Workshop on Singular Optics, Kiev, Ukraine, 24–28 June 2003" *J. Opt. A: Pure Appl. Opt.* **6** (5) (2004)
29. Ilyenkov A V et al., in *15th Intern. Conf. of Coherent and Nonlinear Optics: ICONO'95, June 27–July 1, 1995, St. Petersburg*, Technical Digest, Vol. 1, p. 439
30. Soskin M S, Vasnetsov M V, Basistiy I V, in *15th Intern. Conf. of Coherent and Nonlinear Optics: ICONO'95, June 27–July 1, 1995, St. Petersburg*, Technical Digest, Vol. 2, p. 29
31. Vaupel M, Staliunas K, Weiss C O *Phys. Rev. A* **54** 880 (1996)
32. Rozas D, Law C T, Swartzlander G A *J. Opt. Soc. Am. B* **14** 3054 (1997)
33. Torner L, Petrov D V *J. Opt. Soc. Am. B* **14** 2017 (1997)
34. Desyatnikov A, Denz C, Kivshar Yu *J. Opt. A: Pure Appl. Opt.* **6** S209 (2004)
35. Kivshar Yu S, Agrawal G P *Optical Solitons: from Fibers to Photonic Crystals* (Amsterdam: Academic Press, 2003)
36. Desyatnikov A S, Kivshar Yu S *Phys. Rev. Lett.* **88** 053901 (2002)
37. Ramazza P L, Bortolozzo U, Pastur L *J. Opt. A: Pure Appl. Opt.* **6** S266 (2004)
38. Vinogradova M B, Rudenko O V, Sukhorukov A P *Teoriya Voln* (Theory of Waves) (Moscow: Nauka, 1990)
39. Cycon H L et al. *Schrödinger Operators, with Applications to Quantum Mechanics and Global Geometry* (Eds W Beiglböck et al.) (Berlin: Springer-Verlag, 1987) [Translated into Russian (Moscow: Mir, 1990)]
40. Titchmarsh E C *The Theory of Functions* 2nd ed. (London: Oxford Univ. Press, 1958) [Translated into Russian (Moscow: Nauka, 1980)]
41. Lelong P, Gruman L *Entire Functions of Several Complex Variables* (Berlin: Springer-Verlag, 1986) [Translated into Russian (Moscow: Mir, 1989)]
42. Abramochkin E G, Ph.D. Thesis (Samara: Samara State Teacher's Training Univ., 1996)
43. Fedoryuk M V *Asimptotika: Integraly i Ryady* (Asymptotics: Integrals and Series) (Moscow: Nauka, 1987)
44. Rabinovich Yu L, in *Issledovaniya po Sovremennym Problemam Teorii Funktsii Kompleksnogo Peremennogo* (Investigations on Modern Problems of the Theory of Functions of a Complex Variable) (Ed. A I Markushevich) (Moscow: Fizmatgiz, 1961) p. 186
45. Abramochkin E, Volostnikov V *Opt. Commun.* **102** 336 (1993)
46. Volostnikov V G, Doctoral Thesis (Saratov: Saratov State Univ., 1997)

47. Durnin J *J. Opt. Soc. Am. A* **4** 651 (1987)
48. Davydov A S *Kvantovaya Mekhanika* (Quantum Mechanics) (Moscow: Fizmatgiz, 1963) [Translated into English (Oxford: Pergamon Press, 1965)]; Blokhintsev D I *Osnovy Kvantovoĭ Mekhaniki* (Principles of Quantum Mechanics) (Moscow: Vysshaya Shkola, 1963) [Translated into English (Boston: Allynand Bacon, 1964)]
49. Khapalyuk A P, Doctoral Thesis (Minsk: Belarusian State Univ., 1987)
50. Abramochkin E G *Vestn. Sam. Gos. Univ.: Estestvennonauchn. Ser.* (4) 19 (2001); Abramochkin E G, Volostnikov V G *J. Opt. A: Pure Appl. Opt.* **6** S157 (2004)
51. Wünsche A *J. Opt. Soc. Am. A* **6** 1320 (1989)
52. Indebetouw G *J. Mod. Opt.* **40** 73 (1993)
53. de Broglie L *Les Incertitudes de Heisenberg et l'Interpretation Probabiliste de la Mecanique Ondulatoire* (Paris: Gauthier-Villars, 1982) [Translated into Russian (Moscow: Mir, 1986)]
54. Landau L D, Lifshitz E M *Kvantovaya Mekhanika. Nerelyativistskaya Teoriya* (Quantum Mechanics: Non-Relativistic Theory) (Moscow: Nauka, 1989) [Translated into English (Oxford: Pergamon Press, 1977)]
55. Anan'ev Yu A *Opticheskie Rezonatory i Lazernye Puchki* (Optical Resonators and Laser Beams) (Moscow: Nauka, 1990)
56. Abramochkin E, Volostnikov V *Opt. Commun.* **83** 123 (1991)
57. Gerrard A, Burch J M *Introduction to Matrix Methods in Optics* (New York: Wiley, 1975) [Translated into Russian (Moscow: Mir, 1978)]
58. Abramochkin E, Losevsky N, Volostnikov V *Opt. Commun.* **141** 59 (1997)
59. Abramochkin E, Volostnikov V *Opt. Commun.* **125** 302 (1996)
60. Perelomov A M *Obobshchennye Kogerentnye Sostoyaniya i Ikh Primeneniya* (Generalized Coherent States and Their Applications) (Moscow: Nauka, 1987) [Translated into English (New York: Springer-Verlag, 1986)]; Dodonov V V, Kurmyshev E V, Man'ko V I *Tr. Fiz. Inst. Akad. Nauk SSSR* **176** 128 (1986) [*Proc. Lebedev Phys. Inst.* **176** 169 (1988)]
61. Fuchs D *Kvant* (1) 2 (1979)
62. Geiler V A *Algebra Analiz* **3** (3) 1 (1991) [Translated into English: *St. Petersburg Math. J.* **3** 489 (1992)]
63. Whittaker E T, Watson G N *A Course of Modern Analysis* Vol. 2 (Cambridge: Cambridge Univ. Press, 1952) [Translated into Russian (Moscow: Nauka, 1963)]
64. Bastian M J *Proc. IEEE* **68** 538 (1980); Kuznetsova T I *Kvantovaya Elektron.* **21** 341 (1994) [*Quantum Electron.* **24** 318 (1994)]
65. Volostnikov V G, Loktev M Yu *Opt. Spektrosk.* **86** 80 (1999) [*Opt. Spectrosc.* **86** 69 (1999)]
66. Goncharskiĭ A V, Popov V V, Stepanov V V *Vvedenie v Komp'yuternuyu Optiku* (Introduction to Computer Optics) (Moscow: Izd. MGU, 1991)
67. Vorontsov M A, Matveev A N, Sivokon' V P, in *Komp'yuternaya Optika* (Computer Optics) No. 1 (Samara: Izd. Samarskogo Gos. Aerokosmich. Universiteta, 1987) p. 74
68. Goncharskiĭ A V et al. *Dokl. Akad. Nauk SSSR* **273** 605 (1983) [*Sov. Phys. Dokl.* **28** 955 (1983)]
69. Goncharskiĭ A V, Sisakyan I N, Stepanov V V *Dokl. Akad. Nauk SSSR* **279** 68 (1984)
70. Gerchberg R W, Saxton W O *Optik* **35** 237 (1972)
71. Abramochkin E G, Volostnikov V G, in *Komp'yuternaya Optika* (Computer Optics) No. 10–11 (Samara: Izd. Samarskogo Gos. Aerokosmich. Universiteta, 1992) p. 95
72. Yariv A *Kvantovaya Elektronika* (Quantum Electronics) (Moscow: Sov. Radio, 1980) [Translated into English (New York: Wiley, 1989)]
73. Allen L et al. *Phys. Rev. A* **45** 8185 (1992)
74. Soskin M S et al. *Phys. Rev. A* **56** 4064 (1997)
75. Arnold V I *Matematicheskie Metody Klassicheskoĭ Mekhaniki* (Mathematical Methods of Classical Mechanics) (Moscow: Nauka, 1974) [Translated into English (New York: Springer-Verlag, 1978)]
76. Abramochkin E G, Volostnikov V G, in *Intern. Conf. on Singular Optics, 5–10 October 1997, Partenit, Ukraine* (Proc. SPIE, Vol. 3487, Ed. M S Soskin) (Bellingham, Wash.: SPIE, 1998) p. 20
77. Astaf'eva N M *Usp. Fiz. Nauk* **166** 1145 (1996) [*Phys. Usp.* **39** 1085 (1996)]
78. Dremin I M, Ivanov O V, Nechitailo V A *Usp. Fiz. Nauk* **171** 465 (2001) [*Phys. Usp.* **44** 447 (2001)]